Design of Type-3 Fuzzy Systems and Ensemble Neural Networks for COVID-19 Time Series Prediction Using a Firefly Algorithm

Patricia Melin [1],*, Daniela Sánchez [1], Juan R. Castro [2] and Oscar Castillo [1]

1   Tijuana Institute of Technology, TecNM, Tijuana 22414, Mexico
2   School of Engineering, UABC University, Tijuana 22390, Mexico
*   Correspondence: pmelin@tectijuana.mx

Abstract: In this work, information on COVID-19 confirmed cases is utilized as a dataset to perform time series predictions. We propose the design of ensemble neural networks (ENNs) and type-3 fuzzy inference systems (FISs) for predicting COVID-19 data. The answers for each ENN module are combined using weights provided by the type-3 FIS, in which the ENN is also designed using the firefly algorithm (FA) optimization technique. The proposed method, called ENNT3FL-FA, is applied to the COVID-19 data for confirmed cases from 12 countries. The COVID-19 data have shown to be a complex time series due to unstable behavior in certain periods of time. For example, it is unknown when a new wave will exist and how it will affect each country due to the increase in cases due to many factors. The proposed method seeks mainly to find the number of modules of the ENN and the best possible parameters, such as lower scale and lower lag of the type-3 FIS. Each module of the ENN produces an individual prediction. Each prediction error is an input for the type-3 FIS; moreover, outputs provide a weight for each prediction, and then the final prediction can be calculated. The type-3 fuzzy weighted average (FWA) integration method is compared with the type-2 FWA to verify its ability to predict future confirmed cases by using two data periods. The achieved results show how the proposed method allows better results for the real prediction of 20 future days for most of the countries used in this study, especially when the number of data points increases. In countries such as Germany, India, Italy, Mexico, Poland, Spain, the United Kingdom, and the United States of America, on average, the proposed ENNT3FL-FA achieves a better performance for the prediction of future days for both data points. The proposed method proves to be more stable with complex time series to predict future information such as the one utilized in this study. Intelligence techniques and their combination in the proposed method are recommended for time series with many data points.

Keywords: time series prediction; COVID-19; confirmed cases; ensemble neural networks; firefly algorithm; type-2; type-3 fuzzy logic

MSC: 03B52; 03E72; 62P30

1. Introduction

The COVID-19 pandemic has had worldwide effects since its origin. The number of confirmed cases worldwide has increased, especially in the different waves that each country has experienced. Studies regarding this disease and its repercussions have not ceased since it emerged, which has led to various publications focused on who the people at risk of developing severe COVID-19 are [1,2], the consequences seen in people who were infected with this disease, and the prediction of future cases in order to formulate measures to mitigate the increase in cases [3]. The possibility of developing severe COVID-19 depending on whether a person has other illnesses or is a pregnant woman has been studied [4,5], and the use of drugs and their effects have also been widely studied [1,6]. There is a significant number of models that have been successfully applied to the prediction

and detection of COVID-19 cases. Among these models are those based on the statistics and neural networks applied to time series and human body images [7,8]. In this work, a combination of three techniques is developed: ensemble neural networks, type-3 fuzzy logic, and a firefly algorithm. Each of these intelligence techniques has been successfully applied in different applications, and now they are combined to predict confirmed COVID-19 cases.

The main contribution of this work consists of a hybrid approach combining neural networks in an ensemble as well as interval type-3 fuzzy systems for achieving the aggregation of the outputs of the ensemble. In addition, the firefly algorithm is utilized to automate the design of the ensemble and the interval type-3 fuzzy system. We have to mention that there is no previous work in the literature combining ensembles of neural networks with interval type-3 fuzzy systems and optimizing them with the firefly algorithm, which is an indication of the novelty of the proposed ENNT3FL-FA. Finally, the application of the hybrid approach for COVID-19 prediction is also important because of the real-world implications of the pandemic.

The structure of this paper is as follows. A literature review is presented in Section 2. Brief descriptions of the techniques applied to develop the proposed method are presented in Section 3. The description of the proposed method is shown in Section 4. The experimental results achieved are explained in Section 5. The statistical tests are presented in Section 6. The conclusions are presented in Section 7.

2. Literature Review

Some of the models used for predicting COVID-19 cases are statistical models. In [8], a global prediction of confirmed and recovered cases was proposed using different models based on statistical methodology. The authors used a model selection criterion, where the results are better than those achieved with the standard Gaussian autoregressive time series model. In [9], a Bose–Einstein (BE)-based statistical model for predictions of 14 days was proposed using COVID-19 confirmed case data from New York and DKI Jakarta (Indonesia). The authors wanted to provide the necessary information to decide on the social restrictions that should be used to contain the pandemic. Statistical models such as the generalized Waring regression model were proposed in [10] to predict confirmed COVID-19 cases in Senegal. The authors concluded that this model could consider other factors that affect the number of COVID-19 cases, achieving better results than other count regression models.

Intelligence techniques have also proven to play an important role in facing the COVID-19 pandemic. In [11], a comparison of three predictive models based on artificial neural networks was proposed to predict 10 days of confirmed COVID-19 cases and deaths, using information from 03/11/2020 to 01/23/2021. The achieved results show the effectiveness of this intelligence technique in predicting COVID-19 cases. A method using recurrent and convolutional neural networks to predict confirmed COVID-19 cases was proposed in [12]. The model was applied to the seven most affected states in India, and the results demonstrated that hybridization with convolutional neural networks has a better performance than other proposed hybridizations. In [13], an improvement to the grey wolf optimizer to accelerate convergence by using gradient information was proposed to predict COVID-19 cases in the United States of America. The authors applied a Gaussian walk and Lévy flight to improve the exploration and exploitation to avoid trapping in local optima. An improvement of a long short-term memory network was proposed in [14], where the authors show the behavior of the proposed method with a chaotic time series of COVID-19. They demonstrated the effectiveness of their proposed method for COVID-19 cases in Vietnam. Ensemble neural networks (ENNs), an improvement of conventional neural networks, are a useful technique applied to predict future information based on a data period learned by the modules of the ENNs [15–18]. This improvement of conventional neural networks has also been applied to analyze images to detect COVID-19 infections. In [19], an ensemble deep neural network architecture to detect COVID-19 infections from chest computed tomography (CT) images was proposed. The authors proposed different

architectures and developed a localhost application to perform a diagnosis automatically. In [20], a hybrid system was proposed, where a deep neural network ensemble using pre-trained models (VGG, Xception, and ResNet) and using a genetic algorithm to combine an ensemble architecture was used to perform the classification of clustered images of lung lobes. In [21], an ensemble deep learning model was also proposed to predict COVID-19 infection using chest X-ray images. The authors applied different deep learning models, which indicated that a final combination of an ensemble model can provide better results than individual models. Most previously mentioned works focused on predicting a few future days only in a specific country or in a global prediction.

In a previous work [22], ensemble neural networks were implemented to predict COVID-19 cases, and the ENN architectures were designed using a firefly algorithm. To obtain a final prediction, a comparison among the average, type-1, and type-2 FWA integration methods was performed. The achieved results showed a better performance using the type-2 FWA. Type-3 fuzzy logic has been applied to complex problems where it is combined with other techniques, such as learning algorithms for optimization techniques [23,24]. In [25], a deep learning model with type-3 fuzzy logic to produce forecasting of renewable energies was proposed. For this reason, in this work, a type-3 FWA is proposed to compare with a type-2 FWA and to predict 20 future days (from 03/30/2022 to 04/18/2022). The proposed method is tested using confirmed cases from 12 countries: Brazil, China, France, Germany, India, Iran, Mexico, Italy, Spain, Poland, the United States of America, and the United Kingdom. Different from the previous literature, the main contribution presented in this work is the use of type-3 fuzzy logic to combine responses produced by ENNs. In addition, the type-3 fuzzy inference systems (FISs), as well as the ENNs, are optimally designed by using a firefly algorithm, which has not been previously presented in the literature.

3. Intelligence Techniques

The intelligence techniques applied to develop the proposed method are briefly described in this section.

3.1. Artificial Neural Networks

Human beings have many abilities that stand out from other living beings. Among these skills, we have the ability to learn and recognize. These tasks are performed by the human brain, which recognizes and learns complex problems. These processes can be defined as follows: Information is collected using the human senses (for example, sight), and this information is sent to previously trained neurons. The neurons react to the information providing activations. The next step consists of recognizing shapes, for example, letters or numbers [26,27]. These processes described are mimicked by a technique used in artificial intelligence called artificial neural networks (ANNs). This technique is based on the biological neural networks which compose the human brain trying to make a decision as a human would. To mimic the human brain, ANNs are mainly composed of layers: input, hidden, and output layers, with interconnected units called neurons. The ANNs can simulate complex problems by adjusting parameters as the weights, which during the learning process, store knowledge [28–30]. In Figure 1, the illustration of an ANN is presented where the propagation of the information up to the last layer is performed, because the neurons of each layer (input or hidden) are fully connected to the neurons of the next layer [31,32].

An improvement to an individual ANN is to create an ensemble neural network. Ensemble neural networks (ENNs) are composed of several artificial neural networks that learn the same information, creating individual experts in the same task. Each neural network provides results that can be different from each other [17]. A final result is achieved with the answers provided by the neural networks by combining them using an integration technique. In this work, this kind of ANN is applied to obtain an individual prediction, which is then combined with a unit integration to achieve a final prediction [16,18]. In Figure 2, an example of an ENN with three neural networks (modules) is shown.
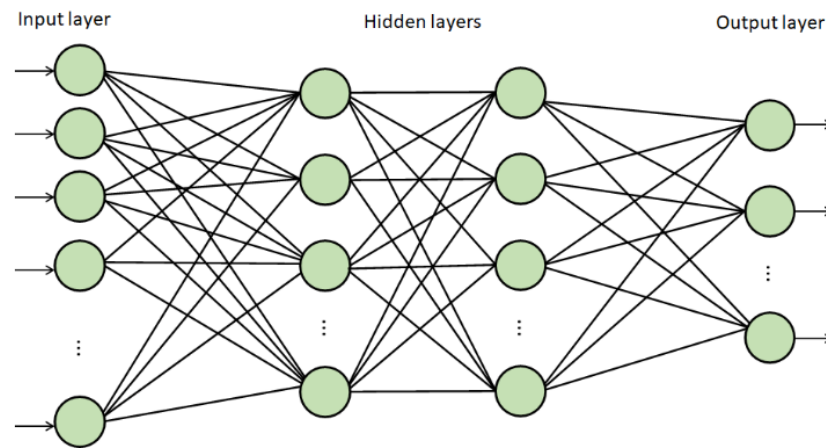
Figure 1. Illustration of an artificial neural network.
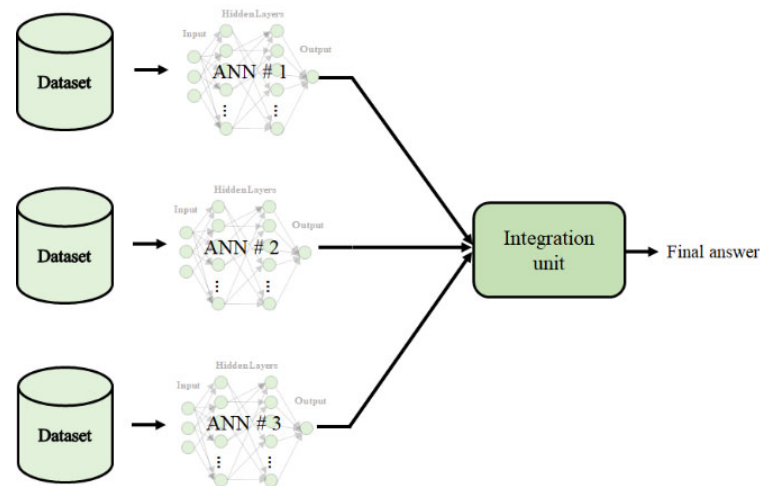
Figure 2. Ensemble neural network.

3.2. Type-3 Fuzzy Logic

In [33], L.A. Zadeh proposed another useful intelligence technique applied to model complex problems: type-1 fuzzy logic (FL), which has a membership as a crisp number in [0, 1]; thus, an element partially belongs with a membership grade to a set. Type-2 FL is proposed in [34], where an element does not have a crisp number between 0 and 1 as in the type-1 FL. In type-2 FL [35–37], the membership function (MF) of an element is defined by a fuzzy set (FS) in [0, 1]. A type-2 FS can be defined as:

$$\tilde{A} = \{((x,u), \mu_{\tilde{A}}(x,u)) \mid \forall_x \in X, \ \forall_u \in J_x \subseteq [0, 1], \ \mu_{\tilde{A}}(x, u) \in [0, 1]\} \qquad (1)$$

where X represents the domain of the fuzzy variable. In this case, there is a primary and a secondary membership. The first one is defined by $J_x \subseteq [0, 1]$, and the second is a type-1 FS defined by $\mu_{\tilde{A}}(x,u)$. The footprint of uncertainty (FOU) is an uncertainty region. If $\mu_{\tilde{A}}(x,u) = 1, \forall_u \in J_x \subseteq [0, 1]$, there is an interval type-2 MF as in Figure 3, where there is a uniform shading of the FOU with its upper $\overline{\mu}_{\tilde{A}}(x)$ and lower $\underline{\mu}_{\tilde{A}}(x)$ MF [38]. An interval type-2 FS is defined as:

$$\tilde{A} = \{((x,u),1) \mid \forall x \in X, \ \forall_u \in J_x \subseteq [0, 1]\} \qquad (2)$$

Figure 3. Gaussian type-2 MF.

A type-3 fuzzy set (T3 FS) [39,40], denoted as $A^{(3)}$, is represented by a trivariate function, called the MF of $A^{(3)}$, in the cartesian product (Equation (3)), wh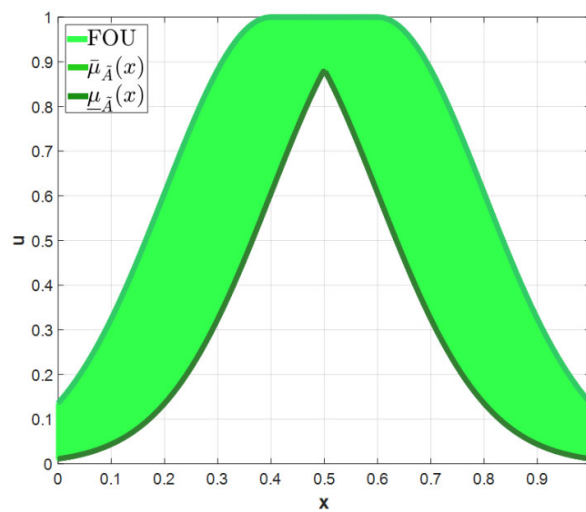ere X is the universe for the primary variable of $A^{(3)}$, x. The MF of $\mu_{A^{(3)}}$ is denoted by $\mu_{A^{(3)}}(x, u, v)$, and is a type-3 MF of the T3 FS:

$$\mu_{A^{(3)}} : X \times [0, 1] \times [0, 1] \to [0, 1] \tag{3}$$

$$A^{(3)} = \left\{ \left(x, u(x), v(x, u), \mu_{A^{(3)}}(x, u, v)\right) \mid x \in X, \; u \in U \subseteq [0, 1], v \in V \subseteq [0, 1] \right\} \tag{4}$$

where for secondary variable u its universe is U, and V for tertiary variable v. A Gaussian interval type-3 MF $\widetilde{\mu}_{\mathbb{A}}(x, u) = $ ScaleGaussScaleGaussIT3MF with Gaussian $FOU(\mathbb{A})$ has parameters $[\sigma, m]$ for the upper membership function (UMF), and for the lower membership function (LMF), λ (lower scale) and ℓ (lower lag), to form the domain of uncertainty $DOU = [\underline{\mu}(x), \overline{\mu}(x)]$. This membership function is represented as:

$$\widetilde{\mu}_{\mathbb{A}}(x, u) = \textbf{ScaleGaussScaleGaussIT3MF} \left(x, \{\{[\sigma, m] \}, \lambda, \ell\}\right) \tag{5}$$

The vertical cuts $\mathbb{A}_{(x)}(u)$ characterize the $FOU(\mathbb{A})$; these are an IT2 FS with a Gaussian IT2 MF, $\mu_{\mathbb{A}_{(x)}}(u)$ with parameters $[\sigma_u, m(x)]$ for the UMF, and for LMF, λ (lower scale) and ℓ (lower lag). This interval type-3 MF is described as:

$$\overline{u}(x) = exp\left[-\frac{1}{2}\left(\frac{x - m}{\sigma}\right)^2\right] \tag{6}$$

$$\underline{u}(x) = \lambda \cdot exp\left[-\frac{1}{2}\left(\frac{x - m}{\sigma^*}\right)^2\right] \tag{7}$$

where $\sigma^* = \sigma \sqrt{\dfrac{\ln(\ell)}{\ln(\varepsilon)}}$, and ε is an epsilon. If $\ell = 0$, $\sigma^* = \sigma$. Then, $\overline{u}(x)$ and $\underline{u}(x)$ are the upper and lower DOU. The range, $\delta(u)$, and radio, σ_u, of the FOU are:

$$\delta(u) = \overline{u}(x) - \underline{u}(x) \tag{8}$$

$$\sigma_u = \frac{\delta(u)}{2\sqrt{3}} + \varepsilon \tag{9}$$

The mean, $m(x)$, of the IT3 MF $\tilde{\mu}(x, u)$ is defined by Equation (10):

$$m(x) = exp\left[-\frac{1}{2}\left(\frac{x-m}{\rho}\right)^2\right] \tag{10}$$

where $\rho = (\sigma + \sigma^*)/2$. Then, the vertical cuts with the IT2 MF, $\mu_{\mathbb{A}(x)}(u) = \left[\underline{\mu}_{\mathbb{A}(x)}(u), \overline{\mu}_{\mathbb{A}(x)}(u)\right]$, are described for Equations (11) and (12):

$$\overline{\mu}_{\mathbb{A}(x)}(u) = exp\left[-\frac{1}{2}\left(\frac{u-u(x)}{\sigma_u}\right)^2\right] \tag{11}$$

$$\underline{\mu}_{\mathbb{A}(x)}(u) = \lambda \cdot exp\left[-\frac{1}{2}\left(\frac{u-u(x)}{\sigma_u^*}\right)^2\right] \tag{12}$$

where $\sigma_u^* = \sigma_u\sqrt{\frac{\ln(\ell)}{\ln(\varepsilon)}}$. If $\ell = 0$, then $\sigma_u^* = \sigma_u$. Then, $\overline{\mu}_{\mathbb{A}(x)}(u)$ and $\underline{\mu}_{\mathbb{A}(x)}(u)$ are the UMF and LMF of the vertical cuts with the IT2 FS of the secondary IT2 MF of the IT3 FS [41]. A visualization of this IT3 MF is shown in Figure 4.
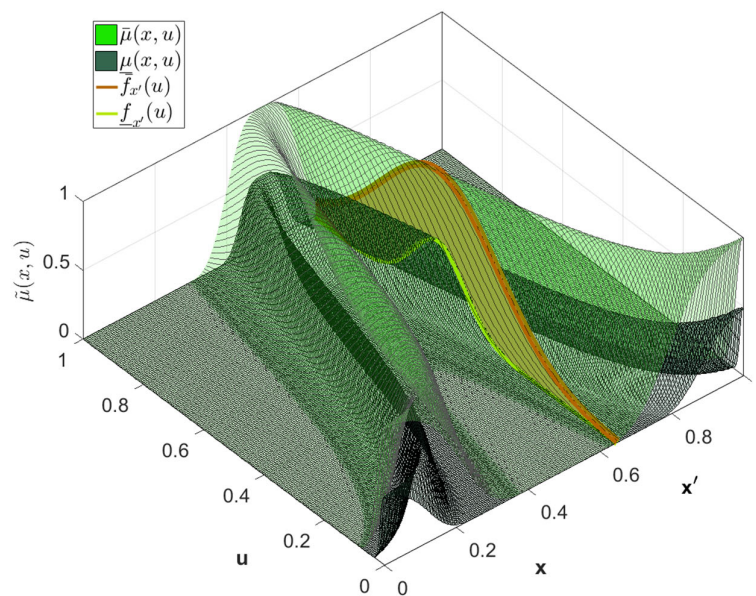
Figure 4. Gaussian type-3 MF.

3.3. Firefly Algorithm

The firefly algorithm (FA) was proposed by Xin-She Yang in [42]. The algorithm is based on the behavior and flashing produced by fireflies. The development of this algorithm is mainly based on three principles: (1) The fireflies do not have sex, which means they are unisex, which allows attraction to any other firefly. (2) The attractiveness of a firefly determines its brightness. The evaluation of a firefly mate includes that the firefly with less brightness is moved in the direction of the other brighter one. Their movement is random if both have the same brightness. (3) The brightness of each firefly is established by the fitness function. In [43], the variation of attractiveness β using the distance *r* is proposed, calculated by:

$$\beta = \beta_0 e^{-\gamma r^2} \tag{13}$$

The attractiveness at $r = 0$ is determined by β_0. The movement in the next iteration of a firefly *i* to the brighter one *j* is calculated by:

$$x_i^{t+1} = x_i^t + \beta_0 e^{-\gamma r_{ij}^2}\left(x_j^t - x_i^t\right) + \alpha_t \varepsilon_i^t \tag{14}$$

where x_i represents a firefly i in the iteration t. The attractiveness of a mate in a group of fireflies is represented with $\beta_0 e^{-\gamma r_{ij}^2}\left(x_j^t - x_i^t\right)$, and ε_i^t is a vector. This vector contains random numbers, α_t, which determine a randomization parameter. The initial randomness scaling factor is given by:

$$\alpha_t = \alpha_t \delta^t \tag{15}$$

where δ is a value [0, 1]. In this work, a random array is implemented to avoid the local minimum; this allows the movement of fireflies to avoid stagnation.

4. Proposed Method

The implementation of the proposed method and dataset are described in this section.

4.1. Proposed Method Description

The proposed method designs ENNs for a time series prediction, where each individual neural network provides a prediction for the testing set and 20 future days. The set of predictions is combined using a type-3 FIS to establish a weight for each prediction, and thus, obtain a final prediction. An FA is applied to design the architecture and parameters of the ENNs and the FIS. The proposed ENNT3FL-FA is shown in Figure 5. The design of each ENN consists of mainly finding the number of modules (ANNs); this task is developed by the FA, which can search from 1 to "m" modules, and each prediction is combined using a type-3 FIS. The firefly algorithm also optimizes the type-3 fuzzy inference system.
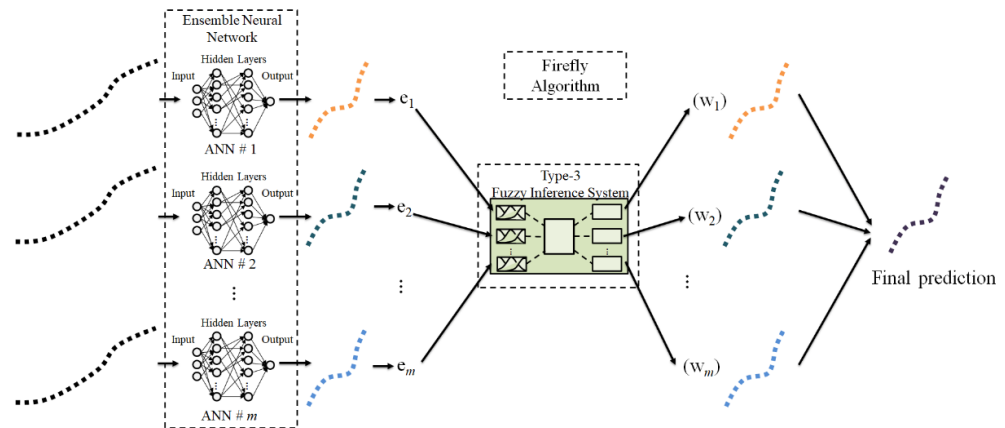
Figure 5. The proposed ENNT3FL-FA.

4.1.1. Description of the ENN

For the ENN establishment, three kinds of ANNs, including function fitting [44], feedforward [45,46], and cascade-forward [47,48] neural networks, can be chosen. Each ENN can be designed using from 1 to "m" neural networks (modules), and this value is established using the FA. In the learning phase, a backpropagation algorithm widely applied to times-series predictions is used: the Levenberg–Marquardt (LM) algorithm, with three feedback delays [22,49]. The calculation of the prediction error of the module k, where $k = \{1, 2, 3, \ldots, m\}$, is given by:

$$MSE_k = \frac{1}{N}\sum_{i=1}^{N}\left(y_i - \hat{y}_{ki}\right)^2 \tag{16}$$

where the real prediction in the time i is represented by y_i. The prediction in the same time provided by the neural network k is represented by $\hat{y}_{ki}$. The number of data points is represented by N.

The ENN design consists mainly of the number (m), and the type of ANN to form the ENN. For each neural network, the goal error, number of hidden layers, and neurons are also sought by the firefly algorithm.

4.1.2. Description of the Type-3 FWA Integration

The prediction error of each ANN is used to obtain a weight to finally produce a final prediction. The weights used to achieve a final prediction are obtained using a Sugeno type-3 FIS model. The design of this FIS is established in two parts: The first one is developed depending on the number of neural networks of the ENN, where the value of "m" (modules or ANNs) determines the input and output number of the FIS. The ranges of each fuzzy input variable, sigma, and mean of three Gaussian type-3 MFs ("low", "medium", and "high") depend on the individual prediction error (MSE). The second part of designing the FIS is determined by the FA, which establishes the values of lower scale and lower lag of the Gaussian type-3 membership functions. In Figure 6, an example of the Sugeno type-3 FIS model is presented.
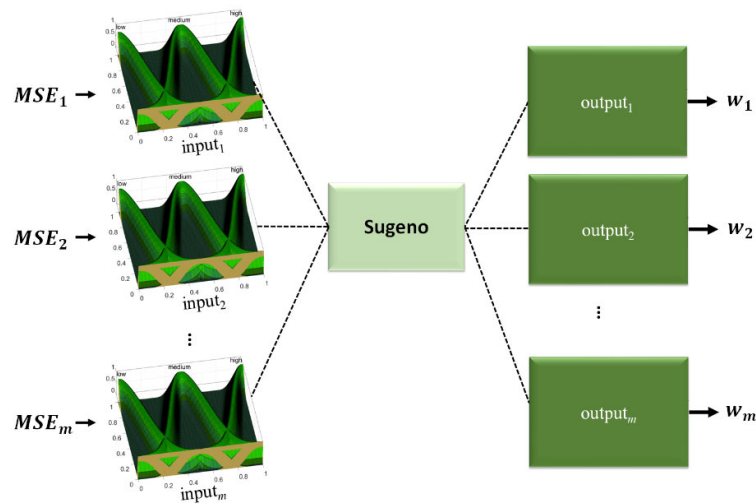
Figure 6. Sugeno type-3 FIS model.

As was previously mentioned, the ranges of the input variables depend on the error prediction (MSE) achieved by each module (normalized value between 0 and 1). That means that for each ENN, a type-3 FIS is designed. The minimal (R_{min}) and maximal (R_{max}) values given by Equations (17) and (18) allow us to define the range of the input variables.

$$R_{min} = \min(MSE_1, MSE_2, MSE_3, \dots, MSE_m) \tag{17}$$

$$R_{max} = \max(MSE_1, MSE_2, MSE_3, \dots, MSE_m) \tag{18}$$

An example of a type-3 fuzzy input variable is shown in Figure 7. As previously mentioned, a Gaussian type-3 membership function has four values: sigma (σ), mean (m), lower scale (λ), and lower lag (ℓ). The difference between R_{min} and R_{max} must be calculated by Equation (19) to determine the sigma and mean values. The sigma value and means of the three membership functions are given by Equations (20)–(23). The constant values of the fuzzy output variables are established by the FA.

$$\mathbf{R_{dif} = R_{max} - R_{min}} \tag{19}$$

$$\sigma = R_{dif} * 0.2 \tag{20}$$

$$m_1 = R_{min} \tag{21}$$

$$m_2 = \left(\frac{R_{dif}}{2}\right) \tag{22}$$

$$m_3 = R_{max} \tag{23}$$
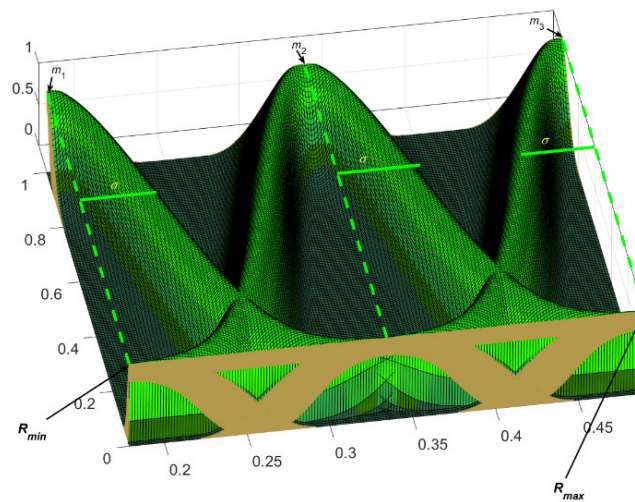
Figure 7. Example of type-3 fuzzy input variable.

Another essential element of an FIS is its fuzzy if-then rules, which allow combining all the predictions based on their errors. In this work, the total number of rules is calculated by Equation (24), where each fuzzy variable has three membership functions.

$$FR = 3^m \tag{24}$$

where m is the number of fuzzy input variables. An example with an ENN with three modules ($m = 3$) is shown in Table 1.

Table 1. Fuzzy if-then rules for three inputs and outputs.

Rule	Antecedents			Consequents		
	e_1	e_2	e_3	w_1	w_2	w_3
1	low	low	low	high	high	high
2	low	low	medium	high	high	medium
3	low	low	high	high	high	low
4	low	medium	low	high	medium	high
5	low	medium	medium	high	medium	medium
6	low	medium	high	high	medium	low
7	low	high	low	high	low	high
8	low	high	medium	high	low	medium
9	low	high	high	high	low	low
10	medium	low	low	medium	high	high
11	medium	low	medium	medium	high	medium
12	medium	low	high	medium	high	low
13	medium	medium	low	medium	medium	high
14	medium	medium	medium	medium	medium	medium
15	medium	medium	high	medium	medium	low
16	medium	high	low	medium	low	high
17	medium	high	medium	medium	low	medium
18	medium	high	high	medium	low	low
19	high	low	low	low	high	high

Table 1. *Cont.*

Rule	Antecedents			Consequents		
	e_1	e_2	e_3	w_1	w_2	w_3
20	high	low	medium	low	high	medium
21	high	low	high	low	high	low
22	high	medium	low	low	medium	high
23	high	medium	medium	low	medium	medium
24	high	medium	high	low	medium	low
25	high	high	low	low	low	high
26	high	high	medium	low	low	medium
27	high	high	high	low	low	low

The type-3 FIS has as inputs the MSE values of each module and, as outputs, the weights corresponding to each prediction. These weights are used with the corresponding prediction to calculate a final prediction using the equation:

$$P = \frac{w_1 \hat{y}_1 + w_2 \hat{y}_2 + \cdots + w_m \hat{y}_m}{w_1 + w_2 + \cdots + w_m} \tag{25}$$

where w_1 is the weight for the prediction obtained by ANN #1, w_2 is the weight for the prediction obtained by ANN #2, and so on up to w_m, which is the weight of the prediction obtained by ANN m, $\hat{y}_1$ is the prediction of ANN #1, $\hat{y}_2$ is the prediction of ANN #2, and so on up to $\hat{y}_m$, which is the prediction of ANN (module) m.

The values used by the firefly algorithm as the search space to design the ENN and FIS are shown in Table 2. The search space for the ensemble neural network is established based on previous works applied to time series predictions [15,22].

Table 2. Search space.

	Parameters	Minimum	Maximum
ENN	Modules (m)	2	5
	Hidden Layers (h)	1	5
	Neurons for Each Hidden Layer	1	50
	Goal Error	0.00001	0.001
Type-3 FIS	Lower Scale (λ)	0.1	0.9
	Lower Lag (ℓ)	0.1	0.9
	Constants	0.1	0.9

For each experiment, the firefly algorithm is established with the parameters based on [22,50]. The settings for the FA are 10 fireflies, an alpha (α) with a value of 0.01, a beta (β) with a value of 1, a delta (δ) with a value of 0.97, and 30 maximum iterations. In Figure 8, the flowchart of the optimization technique is illustrated.

The firefly algorithm has as its objective the minimization of error of the final prediction achieved by the ENN, and the objective function is given by:

$$f = \frac{1}{N} \sum_{i=1}^{N} (Y_i - P_i)^2 \tag{26}$$

where the real prediction in the time i is determined by Y_i, the final prediction of the ENN in the same time is determined by P_i, and the number of data points is determined by N.
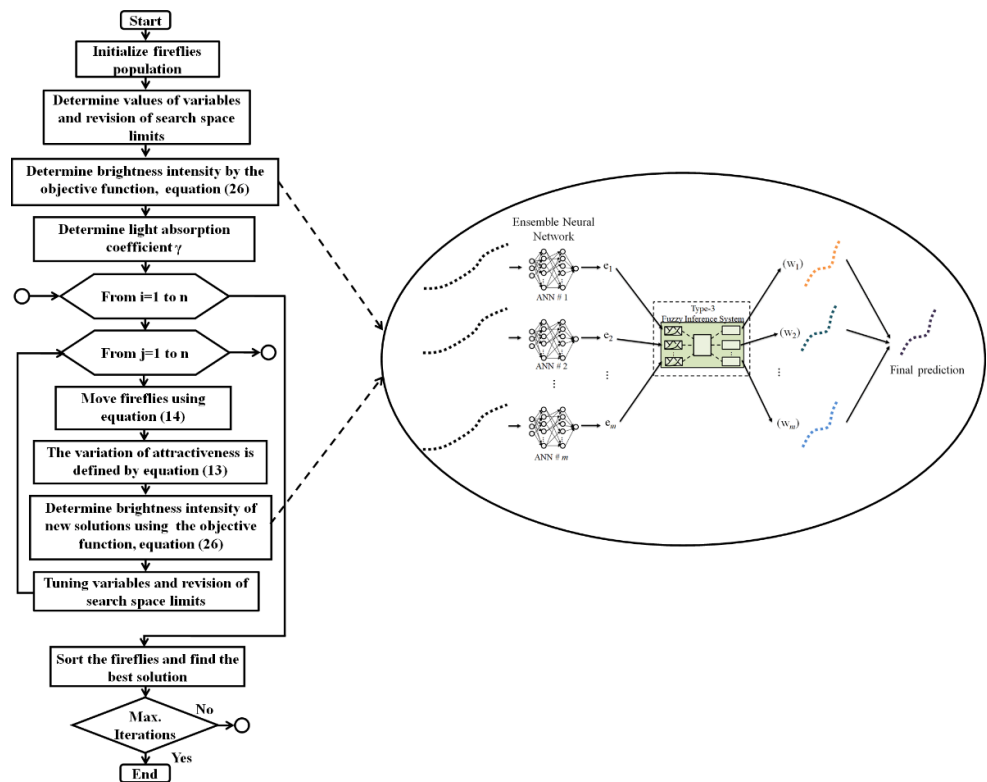
Figure 8. Flowchart of the FA.

4.2. Dataset Description

The information of the worldwide confirmed cases dataset is from the Humanitarian Data Exchange [51]. In this work, two data periods are used to test the performance of the proposed method. Each one is divided into three parts: the testing, training, and validation set. The first data period is from 22 January 2020 to 29 March 2022, and this period consists of 798 days. The second data period consists of 158 days, from 22 January 2020 to 27 June 2020; the results achieved with this second data period are compared with a previous work [22]. For both data periods, 12 countries are analyzed: Brazil, China, France, Germany, India, Iran, Mexico, Italy, Spain, Poland, the United States of America, and the United Kingdom. In Figures 9 and 10, the information by country is shown for the first and second data period, respectively.
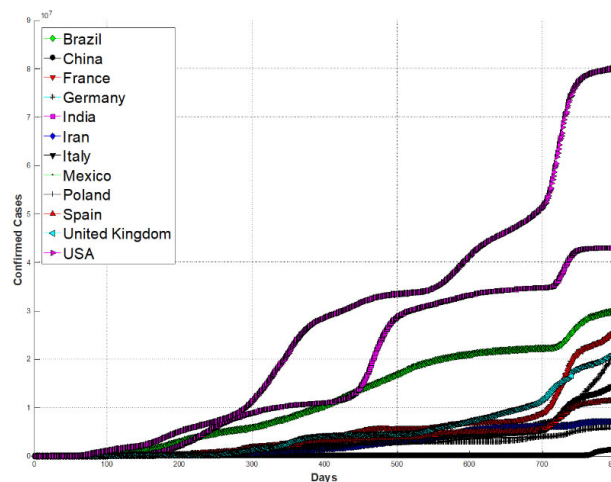
Figure 9. First data period.
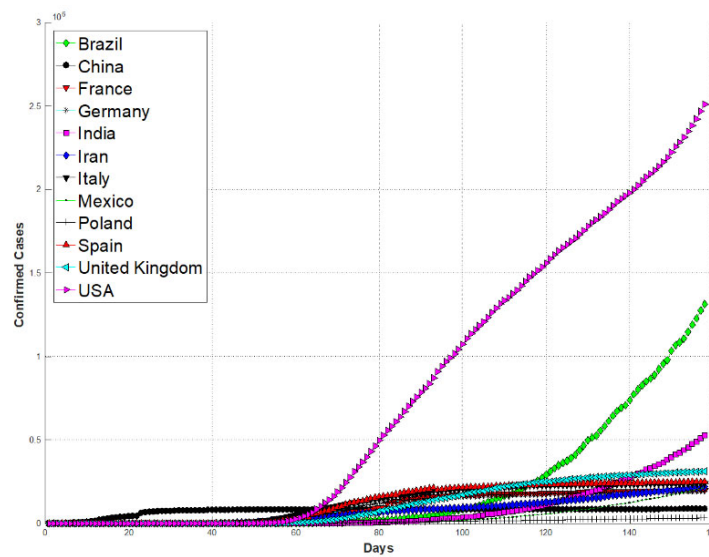
Figure 10. Second data period.

5. Experimental Results

This section presents the results achieved by the proposed method applied to predicting the confirmed cases of 12 countries. The experimental results are achieved using a testing set with 30% of the information (black points on the graphs), leaving 70% to be divided into two sets: training and validation (80/20). Comparisons with a type-2 FWA presented by [22] are performed. As previously mentioned, the information of the confirmed cases of 12 countries is used, with 30 runs performed for each country. An individual prediction of the 20 future days is achieved by each module of the ENN (pink points on the graphs). These predictions are integrated using the weights provided by the FIS, and finally, a final prediction is obtained using Equation (25). This section only shows the results of three countries (Brazil, China, and France) of the first data period, but in Section 4.1 the results of the 12 countries are shown for both data periods.

The ENN architecture, which provides the best future prediction for Brazil, is shown in Table 3. This architecture has three modules using different types of ANNs. The first and second modules use two hidden layers, and the third module only one. The final prediction is obtained using a type-3 FWA.

Table 3. Best architecture for Brazil.

Type	Neurons	Individual (MSE)	Testing (MSE)	Future (MSE)
Feedforward	35, 25	9.58×10^{-7}		
Fitnet	28, 45	1.51×10^{-6}	7.70×10^{-6}	1.84×10^{-6}
Cascade	26	7.49×10^{-7}		

In Figure 11, the individual predictions for the 20 future days and the testing set achieved with the architecture shown in Table 3 for Brazil are shown. In Figure 11b,c, module #2 and module #3 are shown, respectively, where the prediction of the 20 future days (pink points) tends to decrease, but the final integration (Figure 11d) achieved improves its behavior because the first module has a good prediction.

A zoom-in of the best final prediction for Brazil is shown in Figure 12, where the prediction is almost similar to the real behavior. After day #17, the prediction tends to decrease. The type-3 fuzzy input variables generated by the FA are shown in Figure 13 for module #1 (Figure 13a), module #2 (Figure 13b), and module #3 (Figure 13c).

Figure 11. Individual behavior and final prediction for Brazil: (**a**) module #1; (**b**) module #2; (**c**) module #3; (**d**) final prediction.

Figure 12. Best future prediction (Brazil).

In Figure 14, the average convergence obtained by both integration techniques of the 30 runs for Brazil is shown.

The behavior with the type-3 FWA has better convergence than the type-2 FWA technique (testing set). The results achieved with both techniques for the testing set are shown in Table 4, where a better average for Brazil is achieved using the proposed type-3 FWA (indicated in bold in the table).

(a)

(b)

(c)

Figure 13. Type-3 fuzzy input variables (Brazil): (**a**) fuzzy input #1; (**b**) fuzzy input #2; (**c**) fuzzy input #3.
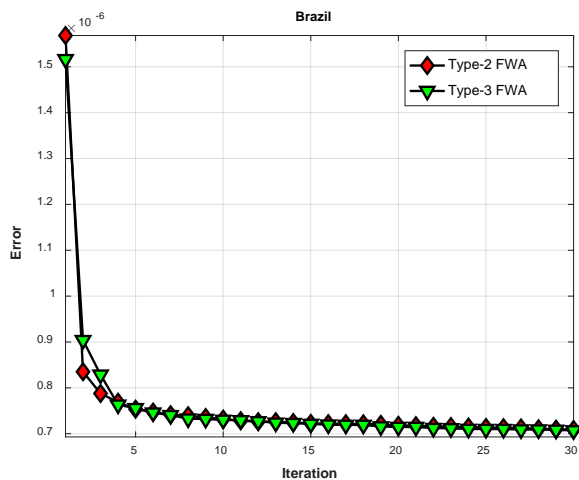
Figure 14. Average convergence for Brazil.

Table 4. First data period (testing prediction, Brazil).

Type-2 FWA			Type-3 FWA		
Best	**Avg**	**Worst**	**Best**	**Avg**	**Worst**
6.88×10^{-7}	7.09×10^{-7}	7.38×10^{-7}	6.90×10^{-7}	$\mathbf{7.07 \times 10^{-7}}$	7.90×10^{-7}

In Figure 15, the average predictions of the 20 future days for Brazil are shown. As these results show, the type-2 and type-3 FWA achieved predictions closer to the real cases up to the eighth day (day #806 6 April 2022). However, after this day, the type-3 FWA integration tends to decrease more than the type-2 FWA. This behavior caused, on average, type-2 to achieve a better performance.

Figure 15. Future prediction (Brazil).

In Table 5, the results of the future prediction for Brazil are shown. These results achieved for Brazil show that type-2 FWA has on average a better performance in a real prediction (indicated in bold in the table).

Table 5. First data period (future prediction, Brazil).

	Type-2 FWA			Type-3 FWA	
Best	**Avg**	**Worst**	**Best**	**Avg**	**Worst**
3.04×10^{-6}	$\mathbf{1.97 \times 10^{-2}}$	1.42×10^{-1}	1.84×10^{-6}	2.46×10^{-2}	1.06×10^{-1}

The ENN architecture, which provides the best future prediction for China, is shown in Table 6. This architecture also has three modules, but each module has only one hidden layer. The final prediction is obtained using the type-3 FWA.

Table 6. Best architecture for China.

Type	Neurons	Individual (MSE)	Testing (MSE)	Future (MSE)
Fitnet	25	3.27×10^{-5}		
Fitnet	28	2.00×10^{-5}	1.40×10^{-5}	5.22×10^{-4}
Feedforward	12	2.15×10^{-4}		

In Figure 16, the individual predictions for the 20 future days and the testing set achieved with the architecture shown in Table 6 for China are shown. The prediction of the 20 future days (pink points) tends to decrease for module #1 (Figure 16a) and module #2 (Figure 16b), but the prediction of module #3 (Figure 16c) achieved a good final integration (Figure 16d).

A zoom-in of the best final prediction for China is shown in Figure 17, where the prediction is almost similar to the real behavior. After day #16, the prediction tends to increase. The type-3 fuzzy input variables generated by the FA are shown in Figure 18 for module #1 (Figure 18a), module #2 (Figure 18b), and module #3 (Figure 18c).
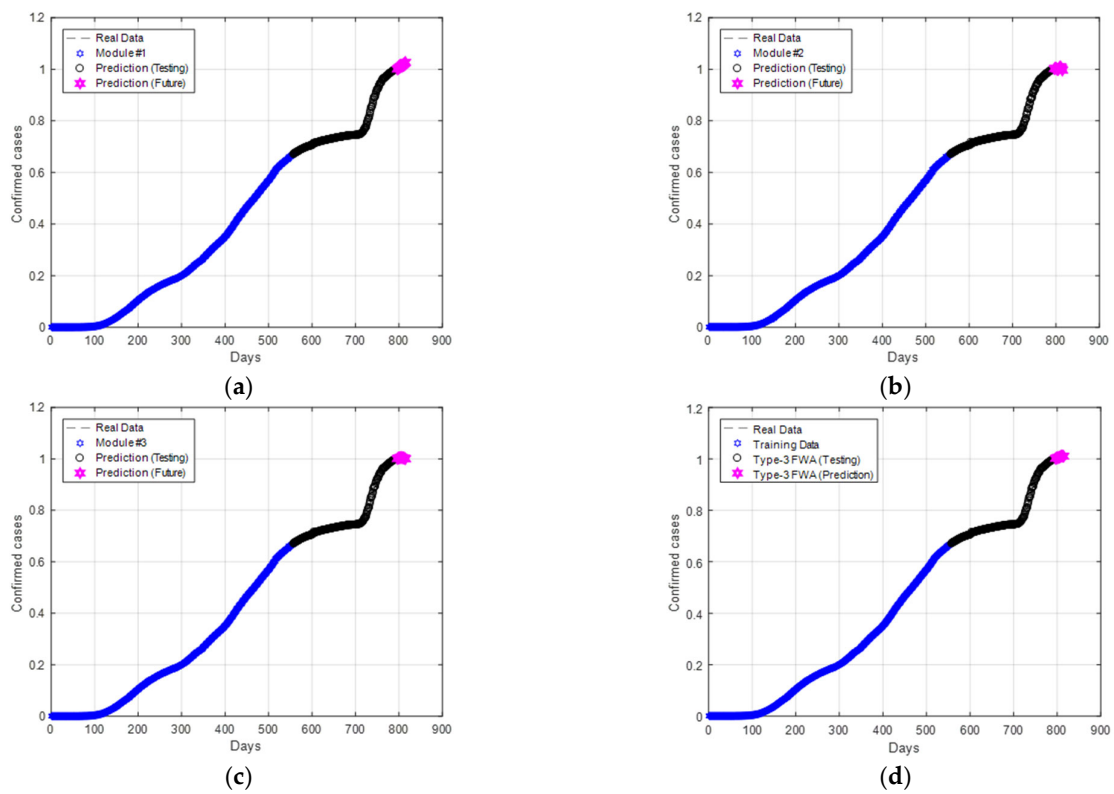
Figure 16. Individual behavior and final prediction for China: (**a**) module #1; (**b**) module #2; (**c**) module #3; (**d**) final prediction.
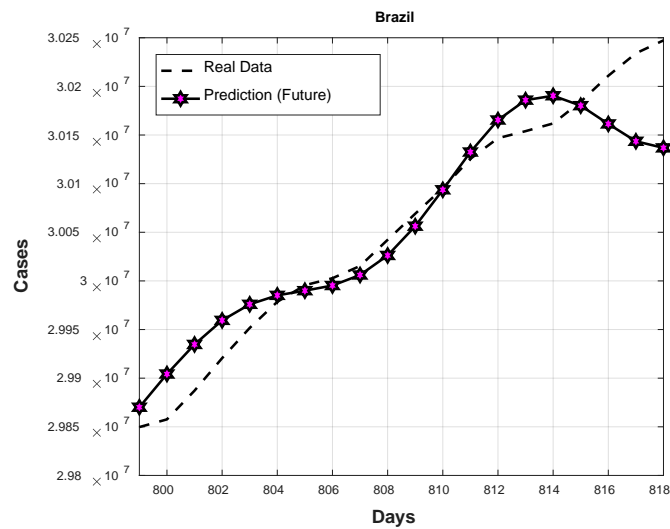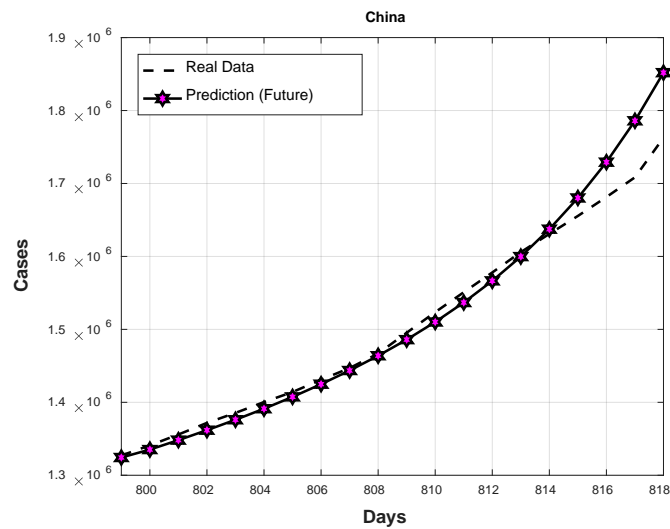

Figure 17. Best future prediction (China).

In Figure 19, the average convergence obtained by both integration techniques of the 30 runs for China is shown. The behavior shown indicates that the type-3 FWA also has better convergence than the type-2 FWA (testing set).

In Table 7, the results achieved with both techniques for the testing set are shown, where a better average for China is achieved using the proposed type-3 FWA (indicated in bold in the table).
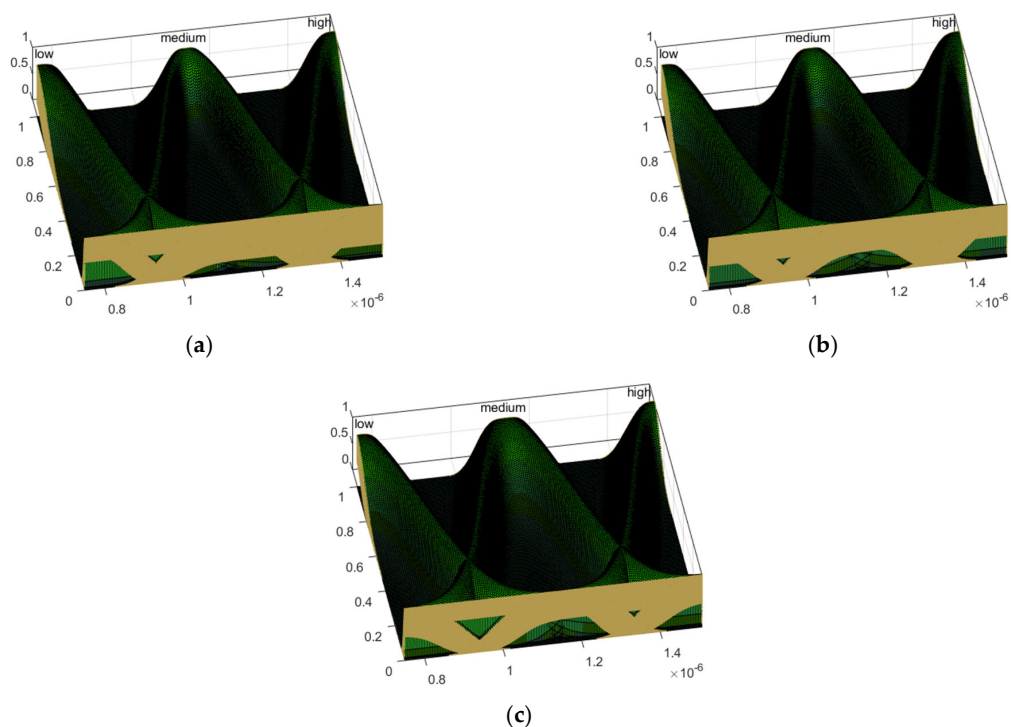
(**a**)

(**b**)

(**c**)

Figure 18. Type-3 fuzzy input variables (China): (**a**) fuzzy input #1; (**b**) fuzzy input #2; (**c**) fuzzy input #3.
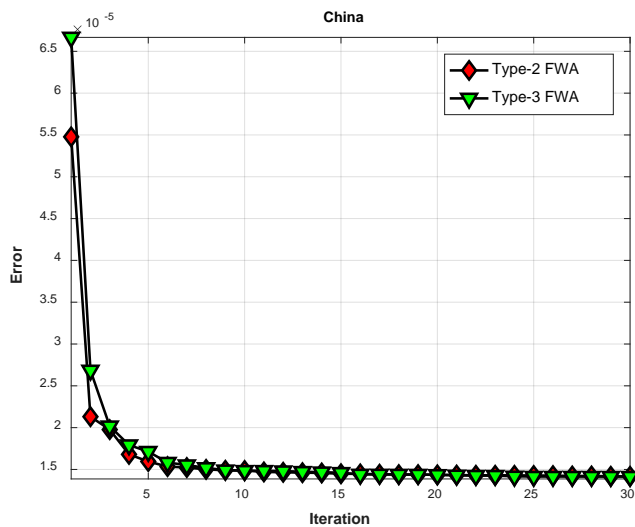
Figure 19. Average convergence for China.

Table 7. First data period (testing prediction, China).

	Type-2 FWA			Type-3 FWA	
Best	**Avg**	**Worst**	**Best**	**Avg**	**Worst**
1.36×10^{-5}	1.42×10^{-5}	1.54×10^{-5}	1.36×10^{-5}	$\mathbf{1.41 \times 10^{-5}}$	1.52×10^{-5}

In Figure 20, the average predictions of the 20 future days for China are shown. The results show that the type-3 FWA achieved predictions closer to the real cases up to the sixteenth day (day #814 14 April 2022). After this day, the type-3 FWA integration had a slight increase.
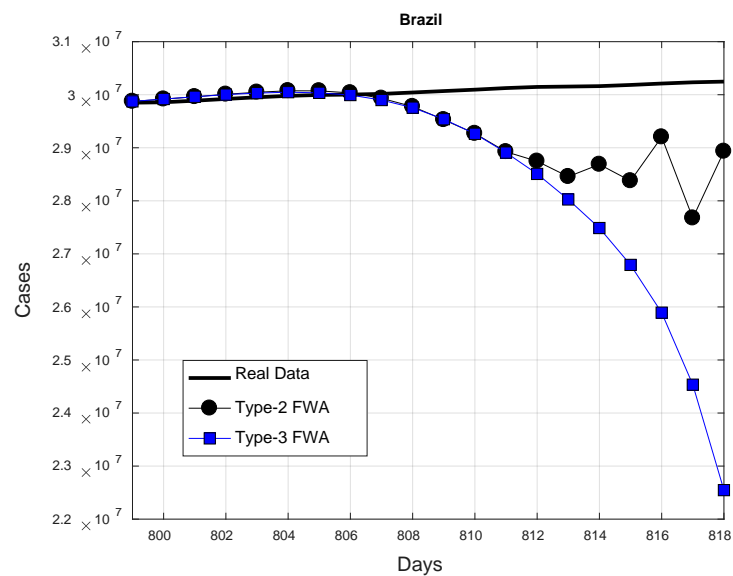
Figure 20. Future prediction (China).

In Table 8, the results of the future prediction for China are shown. These results achieved for China show that the type-3 FWA has on average a better performance in a real prediction (indicated in bold in the table).

Table 8. First data period (future prediction, China).

Type-2 FWA			Type-3 FWA		
Best	**Avg**	**Worst**	**Best**	**Avg**	**Worst**
1.84×10^{-3}	6.98×10^{-2}	2.96×10^{-1}	5.22×10^{-4}	$\mathbf{2.97 \times 10^{-2}}$	1.61×10^{-1}

In Table 9, the ENN architecture, which provides the best future prediction for France, is shown. This architecture has three modules and also uses one hidden layer per module. The final prediction is obtained using the type-3 FWA.

Table 9. Best architecture for France.

Type	Neurons	Individual (MSE)	Testing (MSE)	Future (MSE)
Fitnet	26	6.71×10^{-6}		
Cascade	30	1.34×10^{-5}	6.14×10^{-6}	4.13×10^{-6}
Fitnet	24	9.51×10^{-6}		

In Figure 21, the individual predictions for the 20 future days and the testing set achieved with the architecture shown in Table 9 for France are shown. All the modules achieved a good prediction of the 20 future days (pink points), which allows us to have an excellent final prediction (Figure 21d).

A zoom-in of the best final prediction for France is shown in Figure 22, where the prediction is very similar to the real behavior. The type-3 fuzzy input variables generated by the FA are shown in Figure 23 for module #1 (Figure 23a), module #2 (Figure 23b), and module #3 (Figure 23c).
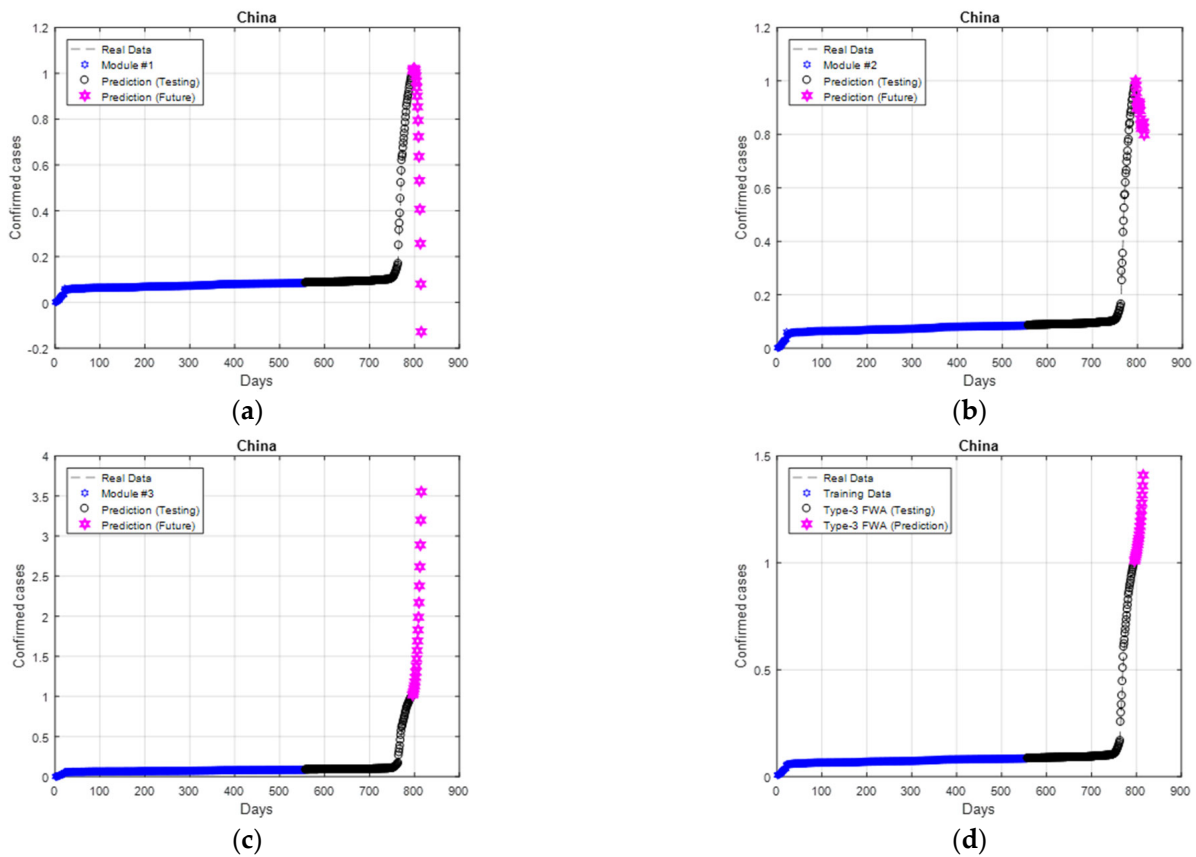
In Figure 24, the average convergence obtained by both integration techniques of the 30 runs for France is shown, where the behavior with the type-2 FWA has better convergence than the type-3 FWA (testing set).
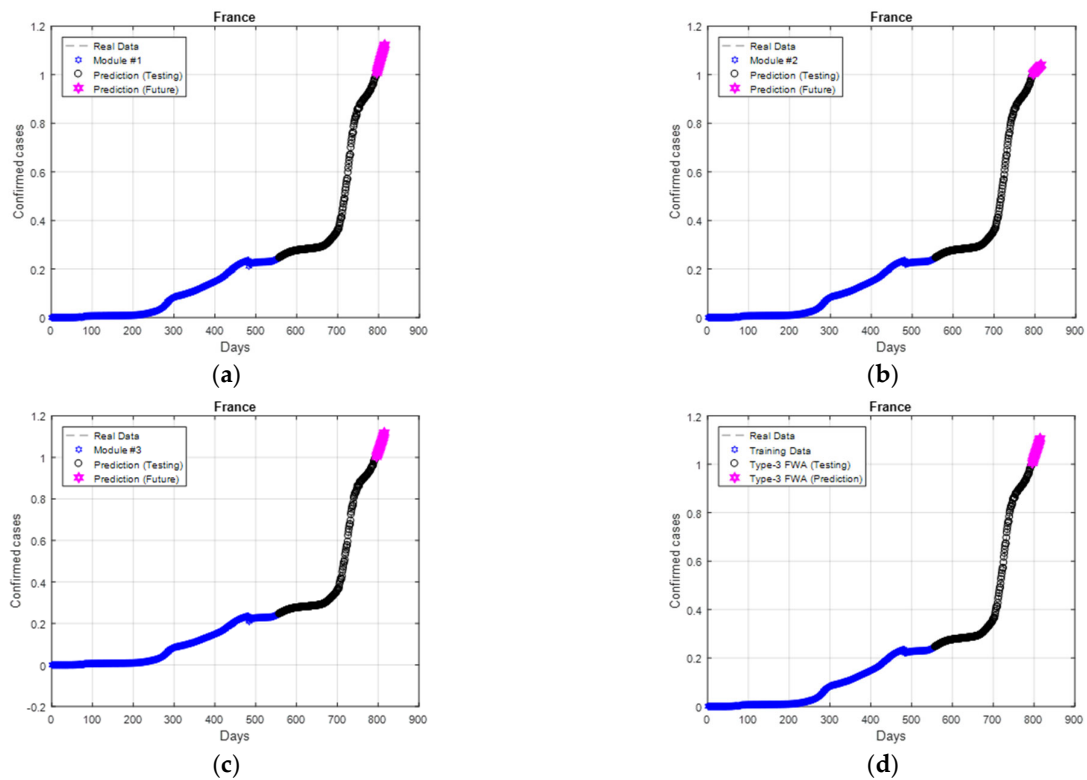
Figure 21. Individual behavior and final prediction for France: (**a**) module #1; (**b**) module #2; (**c**) module #3; (**d**) final prediction.
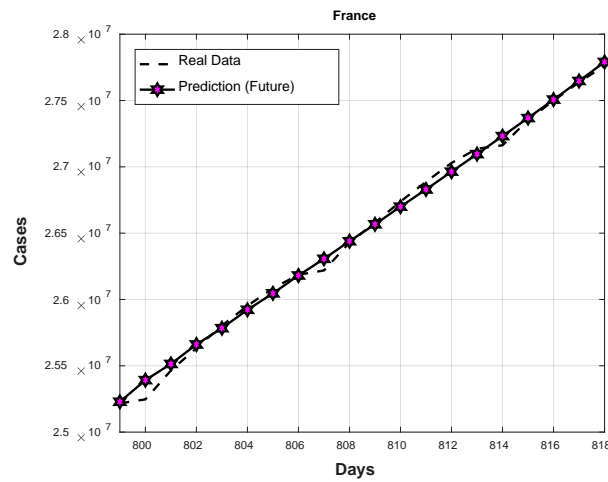
Figure 22. Best future prediction (France).

The results achieved with both techniques for the testing set are shown in Table 10, where a better average for France is achieved using the proposed type-2 FWA (indicated in bold in the table).
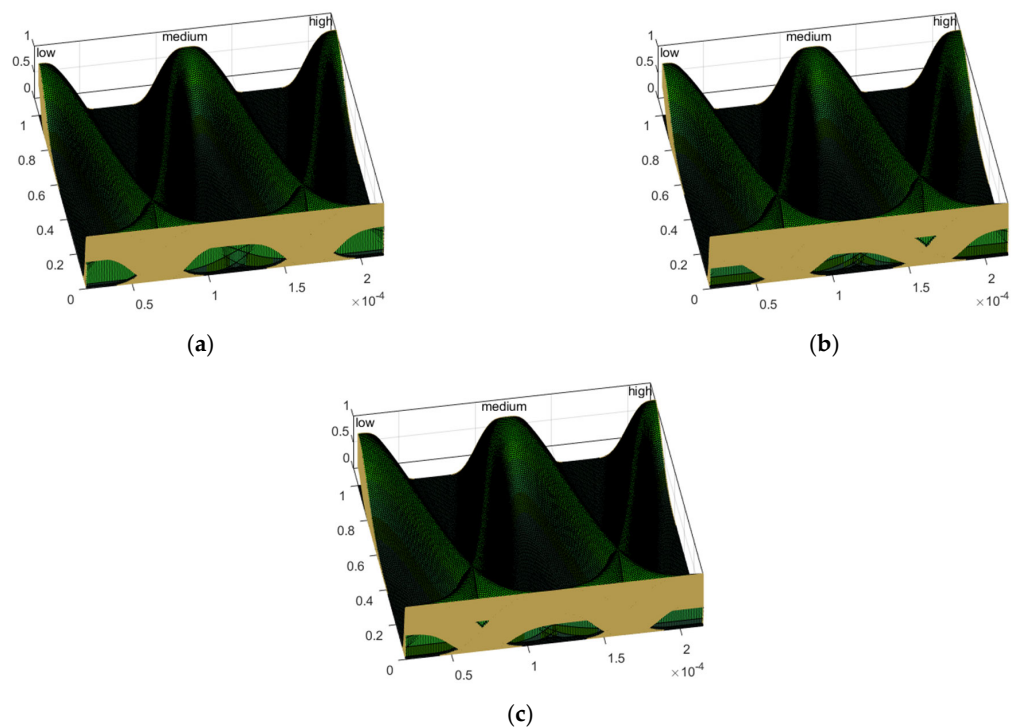
Table 10. First data period (testing prediction, France).

Type-2 FWA			Type-3 FWA		
Best	**Avg**	**Worst**	**Best**	**Avg**	**Worst**
6.09×10^{-6}	$\mathbf{6.25 \times 10^{-6}}$	6.80×10^{-6}	6.14×10^{-6}	6.36×10^{-6}	6.81×10^{-6}

(a)

(b)

(c)
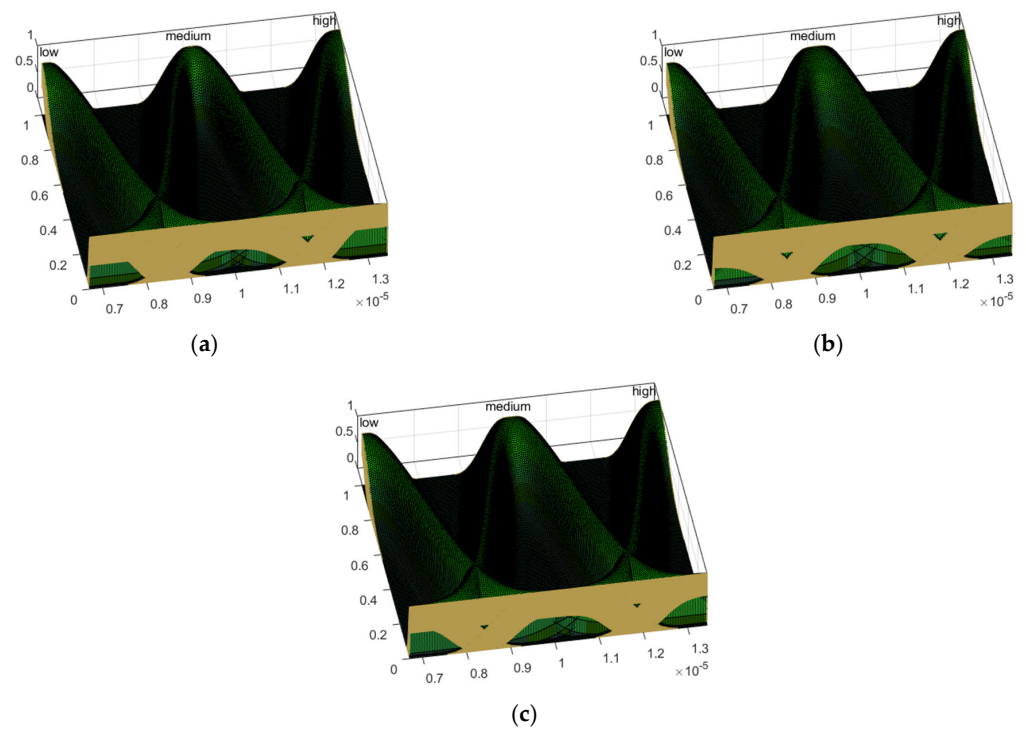
Figure 23. Type-3 fuzzy input variables (France): (**a**) fuzzy input #1; (**b**) fuzzy input #2; (**c**) fuzzy input #3.
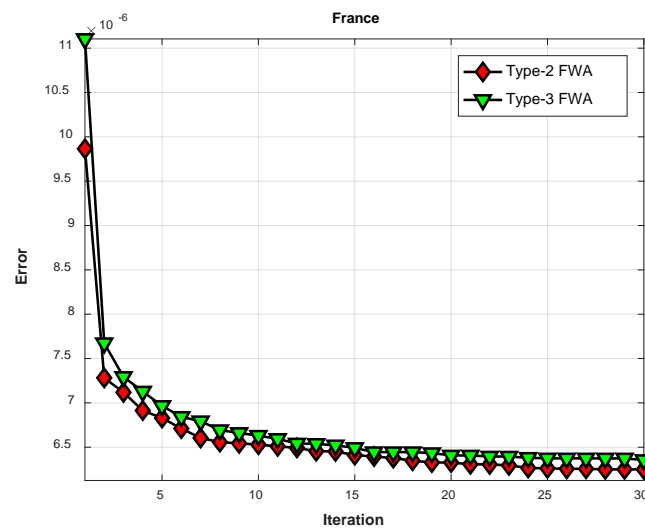
Figure 24. Average convergence for France.

The predictions (averages) for the next 20 days for France are shown in Figure 25. As these results show, the type-3 FWA achieved predictions closer to the real cases up to the seventh day (day #805 5 April 2022). After this day, the type-3 FWA integration tends to increase, but not as much as the type-2 FWA.
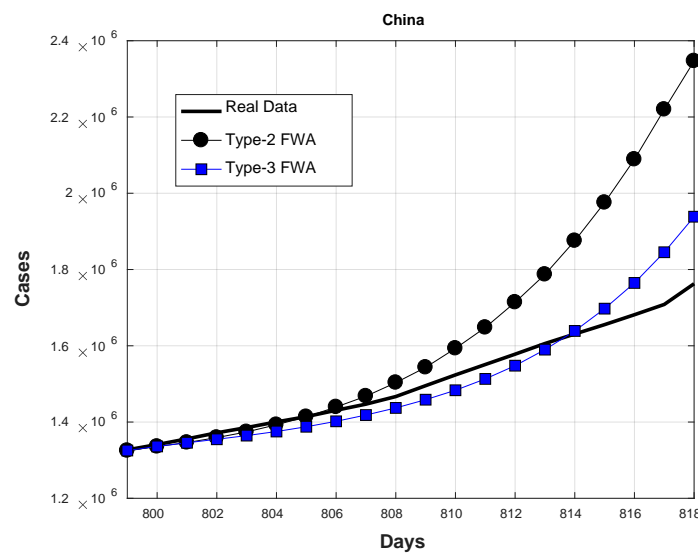
In Table 11, the results of the future prediction for France are shown. These results achieved for France show that the type-3 FWA has on average a better performance in a real prediction (indicated in bold in the table).
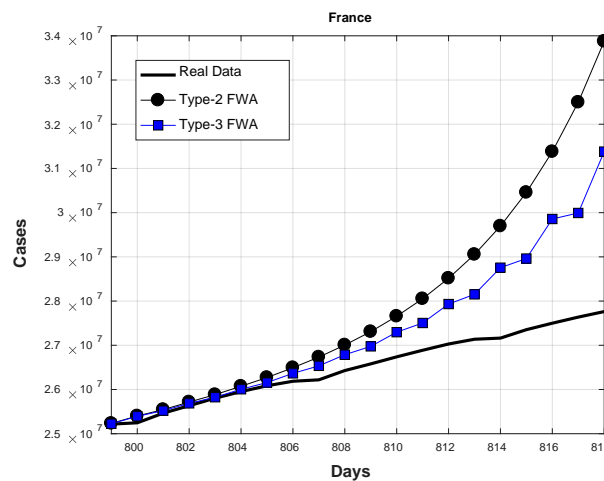
Figure 25. Future prediction (France).

Table 11. First data period (future prediction, France).

	Type-2 FWA			Type-3 FWA	
Best	**Avg**	**Worst**	**Best**	**Avg**	**Worst**
6.07×10^{-6}	2.06×10^{-2}	1.94×10^{-1}	4.13×10^{-6}	**7.11×10^{-3}**	6.06×10^{-2}

Summary of Results

　　The results obtained with the type-3 FWA are presented and compared with the type-2 FWA in this section. The tests were performed using two data periods of confirmed cases of 12 countries. For the testing set for the first data period, the results achieved (MSE) are shown in Table 12. As the results show, the type-2 FWA has on average a better performance for the testing prediction for most countries.

Table 12. First data period (testing prediction).

Country	Type-2			Type-3		
	Best	**Avg**	**Worst**	**Best**	**Avg**	**Worst**
Brazil	6.88×10^{-7}	7.09×10^{-7}	7.38×10^{-7}	6.90×10^{-7}	**7.07×10^{-7}**	7.90×10^{-7}
China	1.36×10^{-5}	1.42×10^{-5}	1.54×10^{-5}	1.36×10^{-5}	**1.41×10^{-5}**	1.52×10^{-5}
France	6.09×10^{-6}	**6.25×10^{-6}**	6.80×10^{-6}	6.14×10^{-6}	6.36×10^{-6}	6.81×10^{-6}
Germany	1.56×10^{-6}	**1.94×10^{-6}**	2.30×10^{-6}	1.61×10^{-6}	2.02×10^{-6}	2.84×10^{-6}
India	4.90×10^{-8}	**5.08×10^{-8}**	5.83×10^{-8}	4.90×10^{-8}	5.14×10^{-8}	5.84×10^{-8}
Iran	2.13×10^{-7}	**2.23×10^{-7}**	2.33×10^{-7}	2.14×10^{-7}	2.28×10^{-7}	2.46×10^{-7}
Italy	2.56×10^{-6}	**2.58×10^{-6}**	2.61×10^{-6}	2.55×10^{-6}	2.59×10^{-6}	2.64×10^{-6}
Mexico	7.27×10^{-6}	**7.28×10^{-6}**	7.30×10^{-6}	7.27×10^{-6}	7.29×10^{-6}	7.32×10^{-6}
Poland	4.55×10^{-7}	**4.60×10^{-7}**	4.98×10^{-7}	4.55×10^{-7}	4.61×10^{-7}	4.78×10^{-7}
Spain	2.20×10^{-5}	**2.21×10^{-5}**	2.22×10^{-5}	2.20×10^{-5}	2.21×10^{-5}	2.23×10^{-5}
United Kingdom	8.42×10^{-6}	8.55×10^{-6}	8.80×10^{-6}	8.36×10^{-6}	**8.54×10^{-6}**	8.79×10^{-6}
USA	2.86×10^{-6}	**2.87×10^{-6}**	2.89×10^{-6}	2.85×10^{-6}	2.88×10^{-6}	2.92×10^{-6}

　　In general, for the future days, the type-3 FWA had on average a better performance based on the results shown in Table 13 (except for Brazil).

Table 13. First data period (future days).

Country	Type-2			Type-3		
	Best	**Avg**	**Worst**	**Best**	**Avg**	**Worst**
Brazil	3.04×10^{-6}	$\mathbf{1.97 \times 10^{-2}}$	1.42×10^{-1}	1.84×10^{-6}	2.46×10^{-2}	1.06×10^{-1}
China	1.84×10^{-3}	6.98×10^{-2}	2.96×10^{-1}	5.22×10^{-4}	$\mathbf{2.97 \times 10^{-2}}$	1.61×10^{-1}
France	6.07×10^{-6}	2.06×10^{-2}	1.94×10^{-1}	4.13×10^{-6}	$\mathbf{7.11 \times 10^{-3}}$	6.06×10^{-2}
Germany	8.02×10^{-4}	8.55×10^{-2}	4.11×10^{-1}	4.09×10^{-5}	$\mathbf{3.02 \times 10^{-2}}$	1.01×10^{-1}
India	1.56×10^{-7}	8.89×10^{-3}	1.54×10^{-1}	3.05×10^{-7}	$\mathbf{3.01 \times 10^{-3}}$	2.05×10^{-2}
Iran	1.12×10^{-5}	1.78×10^{-2}	9.82×10^{-2}	7.56×10^{-7}	$\mathbf{1.43 \times 10^{-2}}$	1.05×10^{-1}
Italy	7.57×10^{-6}	4.54×10^{-2}	2.92×10^{-1}	1.24×10^{-5}	$\mathbf{1.76 \times 10^{-2}}$	8.32×10^{-2}
Mexico	2.86×10^{-5}	9.14×10^{-3}	1.81×10^{-1}	1.48×10^{-5}	$\mathbf{1.49 \times 10^{-3}}$	3.00×10^{-2}
Poland	8.31×10^{-5}	2.05×10^{-2}	4.28×10^{-1}	5.71×10^{-5}	$\mathbf{6.08 \times 10^{-3}}$	5.85×10^{-2}
Spain	5.82×10^{-4}	9.17×10^{-4}	1.54×10^{-3}	5.56×10^{-4}	$\mathbf{8.37 \times 10^{-4}}$	1.54×10^{-3}
United Kingdom	2.80×10^{-5}	7.07×10^{-3}	1.62×10^{-1}	2.69×10^{-4}	$\mathbf{1.26 \times 10^{-2}}$	9.98×10^{-2}
USA	3.15×10^{-6}	8.02×10^{-3}	6.04×10^{-2}	6.26×10^{-7}	$\mathbf{5.32 \times 10^{-3}}$	9.49×10^{-2}

For the first data period, for the testing phase and the next 20 days, the results achieved (averages) are graphically shown in Figures 26 and 27.
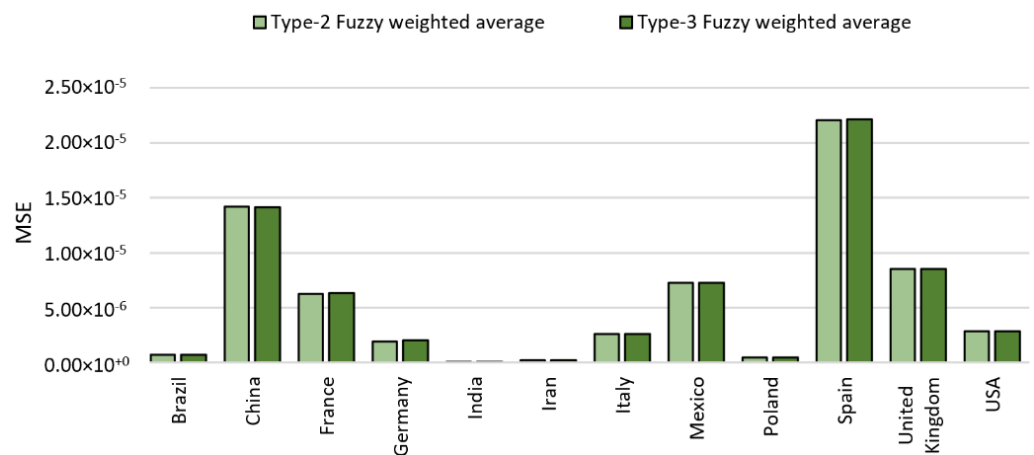

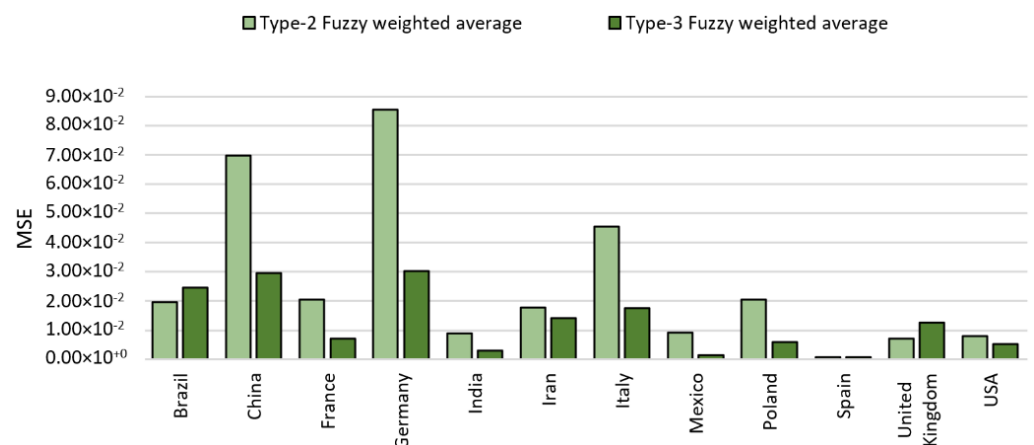**Figure 26.** First data period (testing prediction).

Figure 27. First data period (future prediction).

The results achieved (MSE) for the second data period are shown in Tables 14 and 15. The results achieved with the type-2 FWA were previously presented by [22]. As the results show in Table 15, the testing set with the type-2 FWA has on average a better performance for most countries (eight countries).

Table 14. Second data period (testing prediction).

Country	Type-2			Type-3		
	Best	Avg	Worst	Best	Avg	Worst
Brazil	3.27×10^{-5}	$\mathbf{4.09 \times 10^{-5}}$	4.47×10^{-5}	3.77×10^{-5}	4.17×10^{-5}	4.34×10^{-5}
China	2.40×10^{-8}	$\mathbf{2.66 \times 10^{-8}}$	3.13×10^{-8}	2.31×10^{-8}	2.94×10^{-8}	3.64×10^{-8}
France	2.14×10^{-5}	2.56×10^{-5}	2.94×10^{-5}	2.15×10^{-5}	$\mathbf{2.50 \times 10^{-5}}$	2.76×10^{-5}
Germany	1.90×10^{-6}	$\mathbf{2.00 \times 10^{-6}}$	2.17×10^{-6}	1.85×10^{-6}	2.01×10^{-6}	2.15×10^{-6}
India	1.95×10^{-6}	$\mathbf{2.06 \times 10^{-6}}$	2.36×10^{-6}	1.90×10^{-6}	2.09×10^{-6}	2.29×10^{-6}
Iran	1.40×10^{-6}	$\mathbf{1.47 \times 10^{-6}}$	1.49×10^{-6}	1.43×10^{-6}	$\mathbf{1.48 \times 10^{-6}}$	1.52×10^{-6}
Italy	4.37×10^{-7}	4.55×10^{-7}	4.92×10^{-7}	3.86×10^{-7}	$\mathbf{4.53 \times 10^{-7}}$	4.79×10^{-7}
Mexico	8.13×10^{-6}	8.55×10^{-6}	9.11×10^{-6}	8.19×10^{-6}	$\mathbf{8.53 \times 10^{-6}}$	9.02×10^{-6}
Poland	6.21×10^{-6}	6.76×10^{-6}	6.99×10^{-6}	6.12×10^{-6}	6.75×10^{-6}	6.98×10^{-6}
Spain	2.42×10^{-6}	$\mathbf{2.59 \times 10^{-6}}$	2.64×10^{-6}	2.44×10^{-6}	2.60×10^{-6}	2.64×10^{-6}
United Kingdom	4.97×10^{-6}	$\mathbf{5.93 \times 10^{-6}}$	6.03×10^{-6}	5.87×10^{-6}	5.99×10^{-6}	6.04×10^{-6}
USA	1.50×10^{-6}	$\mathbf{1.52 \times 10^{-6}}$	1.54×10^{-6}	1.50×10^{-6}	1.52×10^{-6}	1.54×10^{-6}

Table 15. Second data period (future days).

Country	Type-2			Type-3		
	Best	Avg	Worst	Best	Avg	Worst
Brazil	8.58×10^{-4}	9.30×10^{-2}	4.50×10^{-1}	9.21×10^{-4}	$\mathbf{6.70 \times 10^{-2}}$	1.60×10^{-1}
China	1.76×10^{-7}	$\mathbf{2.89 \times 10^{-5}}$	2.74×10^{-4}	3.53×10^{-7}	2.43×10^{-4}	5.68×10^{-3}
France	2.42×10^{-5}	$\mathbf{1.33 \times 10^{-3}}$	5.23×10^{-3}	9.87×10^{-6}	1.95×10^{-3}	1.01×10^{-2}
Germany	8.66×10^{-7}	2.04×10^{-4}	1.07×10^{-3}	8.56×10^{-7}	$\mathbf{1.30 \times 10^{-4}}$	8.71×10^{-4}
India	8.38×10^{-4}	1.17×10^{-1}	5.58×10^{-1}	1.07×10^{-4}	$\mathbf{1.12 \times 10^{-1}}$	3.97×10^{-1}
Iran	5.63×10^{-6}	$\mathbf{5.77 \times 10^{-4}}$	1.36×10^{-2}	6.40×10^{-6}	6.91×10^{-4}	1.30×10^{-2}
Italy	1.34×10^{-7}	5.39×10^{-3}	1.43×10^{-1}	2.20×10^{-7}	$\mathbf{2.46 \times 10^{-4}}$	2.63×10^{-3}
Mexico	3.32×10^{-4}	1.09×10^{-1}	6.09×10^{-1}	8.04×10^{-5}	$\mathbf{7.87 \times 10^{-2}}$	4.52×10^{-1}
Poland	7.13×10^{-6}	5.19×10^{-3}	8.62×10^{-2}	8.39×10^{-6}	$\mathbf{2.98 \times 10^{-3}}$	3.88×10^{-2}
Spain	3.88×10^{-6}	1.42×10^{-4}	1.27×10^{-3}	2.12×10^{-6}	$\mathbf{1.15 \times 10^{-4}}$	8.85×10^{-4}
United Kingdom	2.61×10^{-5}	3.62×10^{-4}	2.09×10^{-3}	2.70×10^{-5}	$\mathbf{1.97 \times 10^{-4}}$	7.12×10^{-4}
USA	1.60×10^{-4}	$\mathbf{2.11 \times 10^{-3}}$	6.99×10^{-3}	5.10×10^{-5}	2.44×10^{-3}	8.44×10^{-3}

However, for the future days, most countries (eight countries) had on average a better performance using the type-3 FWA integration.

The results achieved (averages) for the second data period for the testing phase and the next 20 days are graphically shown in Figures 28 and 29.
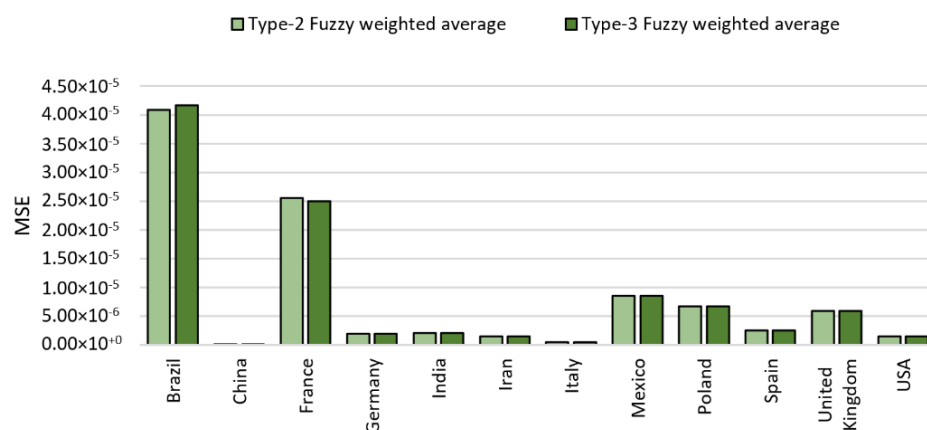
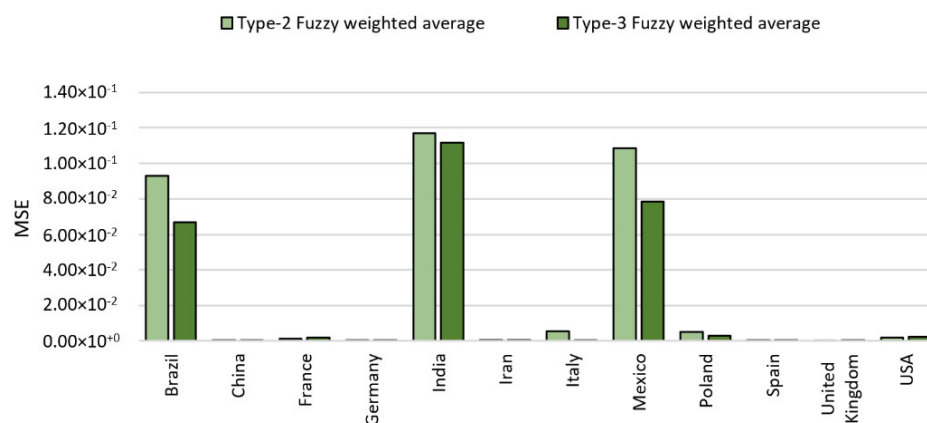**Figure 28.** Second data period (testing prediction).

Figure 29. Second data period (future prediction).

6. Statistical Comparison

The Shapiro–Wilk test was performed on each country for both data periods (testing and future prediction) to determine if the results are normally distributed. Due to the results achieved, where the normality assumption is not passed, a non-parametric test must be applied. The Mann–Whitney tests were performed to compare both integration techniques, where the median is used [52]. The achieved results are presented in this section. In this work, a 0.05 level of significance is utilized to perform the comparisons. The null hypothesis indicates that there is no difference between both techniques. The null hypothesis is rejected if the *p*-value is smaller than 0.05. The lower median for each country is underlined in each table.

The Mann–Whitney results for each country of the first data period for the testing days are shown in Table 16. As the results show (indicated in bold in the table), there is only a significant difference in only two countries (France and Iran) using the type-2 FWA.

Table 17 shows the results for each country of the first data period for the future days. As the results show (indicated in bold in the table), there is only a significant difference in only four countries. The type-2 FWA is significantly different for Brazil and the United Kingdom, and the type-3 FWA for China and Germany. However, the median achieved by the type-3 FWA for other countries was also lower than that the achieved by the type-2 FWA.

Table 18 shows the results for each country of the second data period for the testing days. As the results show (indicated in bold in the table), there is only a significant difference in only three countries (China, Iran, and the United Kingdom) using the type-2 FWA.

Table 16. Mann–Whitney results (first data period, testing prediction).

Country	Median		p-Value
	Type-2	Type-3	
Brazil	7.09×10^{-7}	7.02×10^{-7}	0.0989
China	1.41×10^{-5}	1.40×10^{-5}	0.5892
France	6.22×10^{-6}	6.33×10^{-6}	**0.0094**
Germany	1.94×10^{-6}	2.03×10^{-6}	0.2501
India	5.02×10^{-8}	5.07×10^{-8}	0.5058
Iran	2.23×10^{-7}	2.27×10^{-7}	**0.0251**
Italy	2.58×10^{-6}	2.58×10^{-6}	0.1119
Mexico	7.28×10^{-6}	7.28×10^{-6}	0.1494
Poland	4.58×10^{-7}	4.60×10^{-7}	0.3478
Spain	2.21×10^{-5}	2.21×10^{-5}	0.1236
United Kingdom	8.53×10^{-6}	8.51×10^{-6}	0.4295
USA	2.87×10^{-6}	2.87×10^{-6}	0.0785

Table 17. Mann–Whitney results (first data period, future prediction).

Country	Median		p-Value
	Type-2	Type-3	
Brazil	1.60×10^{-3}	1.05×10^{-2}	**0.0257**
China	5.21×10^{-2}	1.69×10^{-2}	**0.0035**
France	5.84×10^{-3}	9.99×10^{-4}	0.2983
Germany	5.78×10^{-2}	1.98×10^{-2}	**0.0394**
India	2.45×10^{-4}	3.39×10^{-4}	0.9522
Iran	5.42×10^{-3}	3.18×10^{-4}	0.0854
Italy	8.36×10^{-3}	5.97×10^{-3}	0.1902
Mexico	3.50×10^{-4}	2.34×10^{-4}	0.1164
Poland	9.38×10^{-4}	1.03×10^{-3}	0.7414
Spain	8.91×10^{-4}	8.09×10^{-4}	0.1707
United Kingdom	6.06×10^{-4}	2.17×10^{-3}	**0.0048**
USA	2.28×10^{-4}	2.64×10^{-4}	0.3789

Table 18. Mann–Whitney results (second data period, testing prediction).

Country	Median		p-Value
	Type-2	Type-3	
Brazil	4.09×10^{-5}	4.21×10^{-5}	0.2609
China	2.65×10^{-8}	2.97×10^{-8}	**0.0001**
France	2.59×10^{-5}	2.51×10^{-5}	0.1971
Germany	1.99×10^{-6}	2.02×10^{-6}	0.4110
India	2.05×10^{-6}	2.07×10^{-6}	0.1353
Iran	1.47×10^{-6}	1.48×10^{-6}	**0.0166**

Table 18. *Cont.*

Country	Median		*p*-Value
	Type-2	Type-3	
Italy	4.55×10^{-7}	$\underline{4.55} \times 10^{-7}$	0.9920
Mexico	8.51×10^{-6}	$\underline{8.50} \times 10^{-6}$	0.6818
Poland	6.83×10^{-6}	$\underline{6.82} \times 10^{-6}$	0.8999
Spain	2.62×10^{-6}	$\underline{2.62} \times 10^{-6}$	0.5069
United Kingdom	$\underline{5.97} \times 10^{-6}$	6.00×10^{-6}	**0.0071**
USA	$\underline{1.52} \times 10^{-6}$	1.52×10^{-6}	0.8067

In Table 19, the results for each country of the second data period for the future days are shown. As the results show (indicated in bold in the table), no significant difference exists for any country. However, the median values achieved by the type-3 FWA for seven countries were lower than those achieved by the type-2 FWA.

Table 19. Mann–Whitney results (second data period, future prediction).

Country	Median		*p*-Value
	Type-2	Type-3	
Brazil	$\underline{5.72} \times 10^{-2}$	6.70×10^{-2}	0.9920
China	1.19×10^{-5}	$\underline{4.49} \times 10^{-6}$	0.0989
France	$\underline{9.72} \times 10^{-4}$	1.58×10^{-3}	0.3077
Germany	7.64×10^{-5}	$\underline{6.80} \times 10^{-5}$	0.5687
India	$\underline{2.23} \times 10^{-2}$	5.76×10^{-2}	0.7718
Iran	8.83×10^{-5}	$\underline{2.96} \times 10^{-5}$	0.1010
Italy	1.09×10^{-4}	$\underline{4.67} \times 10^{-5}$	0.1052
Mexico	6.84×10^{-2}	$\underline{2.27} \times 10^{-2}$	0.1770
Poland	1.08×10^{-3}	$\underline{1.04} \times 10^{-3}$	0.7263
Spain	$\underline{4.11} \times 10^{-5}$	4.49×10^{-5}	0.4715
United Kingdom	2.64×10^{-4}	$\underline{1.60} \times 10^{-4}$	0.1096
USA	$\underline{2.04} \times 10^{-3}$	2.29×10^{-3}	0.3421

7. Conclusions

This paper utilized the information of confirmed COVID-19 cases to predict the cases of 20 future days. The proposed ENNT3FL-FA combines ENNs, type-3 fuzzy logic, and a firefly algorithm, which was not previously proposed. The firefly algorithm allows us to design optimal ENN architectures and fuzzy inference systems to predict confirmed COVID-19 cases, where each individual prediction obtains a weight using the Sugeno model type-3 fuzzy inference system generated by the firefly algorithm to produce a final prediction. The proposed method was tested using the information of 12 countries in two data periods. The first data period contains information from 798 days, and the second one only 158 days. The last one was used to compare these results with a previous work, where integration techniques such as the average, type-1, and type-2 FWA were compared, and it was found that better results were achieved with the type-2 FWA. For this reason, in this work, the proposed method was compared with the type-2 FWA. The proposed ENNT3FL-FA achieved a better performance on the prediction of future days for both data periods in countries such as Germany, India, Italy, Mexico, Poland, Spain, the United Kingdom, and the United States of America based on the average values. However, when

Mann–Whitney tests were performed, the achieved results showed for the first data period (798 days) in the testing prediction that there is only a significant difference for France and Iran predictions, where the best median values are achieved with the type-2 FWA. A similar situation occurred for the second data period (158 days), also in the testing period, where the type-2 FWA has better median values for Iran and the United Kingdom. For the future prediction, in the case of the first data period, there is a significant difference for Brazil and the United Kingdom predictions, where the best median values are achieved with the type-2 FWA, and only Germany obtained a significant difference by the type-3 FWA. In the second data period, the comparison between the type-2 FWA and the type-3 FWA does not provide significant differences. However, it is important to mention that for both data periods in the future prediction, more countries have lower median values with the proposed ENNT3FL-FA. With the results achieved, we conclude that ENNT3FL-FA provides a better performance in predicting future days and simulates the real behavior for the data period with more information, although statistically only a significant difference is achieved in a few countries. The main challenge of the proposed ENNT3FL-FA is to achieve a better performance with the testing prediction; this would allow for achieving a better future prediction. In future works, other type-3 membership functions will be implemented to evaluate their performance with another data period of COVID-19 and other infectious diseases such as influenza and monkeypox. We also will consider implementing other optimization methods to compare results and performance.

Author Contributions: Methodology and validation, P.M.; software, validation and writing, D.S.; conceptualization, creation of the main idea, and writing—review and editing, O.C.; formal analysis, J.R.C. All authors have read and agreed to the published version of the manuscript.

Data Availability Statement: Not applicable.

Conflicts of Interest: The authors declare no conflict of interest.

References

1. Jin, Z.; Liu, J.Y.; Feng, R.; Ji, L.; Jin, Z.L.; Li, H.B. Drug treatment of coronavirus disease 2019 (COVID-19) in China. *Eur. J. Pharmacol.* **2020**, *883*, 32598953. [CrossRef] [PubMed]
2. Zhang, Q.; Wei, Y.; Chen, M.; Wan, Q.; Chen, X. Clinical analysis of risk factors for severe COVID-19 patients with type 2 diabetes. *J. Diabetes Complicat.* **2020**, *34*, 107666. [CrossRef] [PubMed]
3. Melin, P.; Monica, J.C.; Sánchez, D.; Castillo, O. Analysis of Spatial Spread Relationships of Coronavirus (COVID-19) Pandemic in the World using Self Organizing Maps. *Chaos Solit. Fractals* **2020**, *138*, 109917. [CrossRef] [PubMed]
4. Reddy, D.; Atam, V.; Rai, P.; Khan, F.; Pandey, S.; Malhotra, H.; Gupta, K.; Sonkar, S.; Verma, R.; KGMU COVID-19 Working Group. COVID-19 cases and their outcome among patients with uncommon co-existing illnesses: A lesson from Northern India. *Clin. Epidemiol. Glob. Health* **2022**, *15*, 101044. [CrossRef]
5. Zha, L.; Sobue, T.; Hirayama, A.; Takeuchi, T.; Tanaka, K.; Katayama, Y.; Komukai, S.; Shimazu, T.; Kitamura, T.; COVID-19 Epidemiology Research Group. Characteristics and Outcomes of COVID-19 in Reproductive-Aged Pregnant and Nonpregnant Women in Osaka, Japan. *Int. J. Infect. Dis.* **2022**, *117*, 195–200. [CrossRef]
6. Reyes, L.; Rodriguez, A.; Bastidas, A.; Parra-Tanoux, D.; Fuentes, Y.V.; García-Gallo, E.; Moreno, G.; Ospina-Tascon, G.; Hernandez, G.; Silva, E.; et al. Dexamethasone as risk-factor for ICU-Acquired respiratory tract infections in severe COVID-19. *J. Crit. Care* **2022**, *69*, 154014. [CrossRef]
7. Liu, D.; Ding, W.; Dong, Z.; Pedrycz, W. Optimizing deep neural networks to predict the effect of social distancing on COVID-19 spread. *Comput. Ind. Eng.* **2022**, *166*, 107970. [CrossRef]
8. Maleki, M.; Mahmoudi, M.R.; Wraith, D.; Pho, K.-H. Time series modelling to forecast the confirmed and recovered cases of COVID-19. *Travel Med. Infect. Dis.* **2020**, *37*, 101742. [CrossRef]
9. Halide, H. Predicting COVID-19 confirmed cases in New York and DKI Jakarta by nonlinear fitting of a Bose–Einstein energy distribution and its implications on social restrictions. *Gac. Sanit.* **2021**, *25*, S604–S609. [CrossRef]
10. Gning, L.; Ndour, C.; Tchuenche, J.M. Modeling COVID-19 daily cases in Senegal using a generalized Waring regression model. *Physica A* **2022**, *597*, 127245. [CrossRef]

11. Kuvvetli, Y.; Deveci, M.; Paksoy, T.; Garg, H. A predictive analytics model for COVID-19 pandemic using artificial neural networks. *Decis. Anal.* **2021**, *1*, 1–13. [CrossRef]
12. Verma, H.; Mandal, S.; Gupta, A. Temporal deep learning architecture for prediction of COVID-19 cases in India. *Expert Syst. Appl.* **2022**, *195*, 116611. [CrossRef] [PubMed]
13. Khalilpourazari, S.; Doulabi, H.; Çiftçioglu, A.; Weber, G. Gradient-based grey wolf optimizer with Gaussian walk: Application in modelling and prediction of the COVID-19 pandemic. *Expert Syst. Appl.* **2021**, *177*, 114920. [CrossRef] [PubMed]
14. Pham, P.; Pedrycz, W.; Vo, B. Dual attention-based sequential auto-encoder for Covid-19 outbreak forecasting: A case study in Vietnam. *Expert Syst. Appl.* **2022**, *203*, 117514. [CrossRef]
15. Pulido, M.; Melin, P.; Castillo, O. Particle swarm optimization of ensemble neural networks with fuzzy aggregation for time series prediction of the Mexican Stock Exchange. *Inf. Sci.* **2014**, *280*, 188–204. [CrossRef]
16. Melin, P.; Monica, J.C.; Sánchez, D.; Castillo, O. Multiple Ensemble Neural Network Models with Fuzzy Response Aggregation for Predicting COVID-19 Time Series: The Case of Mexico. *Healthcare* **2020**, *8*, 181. [CrossRef]
17. Jia, D.; Wu, Z. Seismic fragility analysis of RC frame-shear wall structure under multidimensional performance limit state based on ensemble neural network. *Eng. Struct.* **2021**, *246*, 112975. [CrossRef]
18. Wilkinson, I.; Bhattacharjee, R.; Shafer, J.; Osborne, A. Confidence estimation in the prediction of epithermal neutron resonance self-shielding factors in irradiation samples using an ensemble neural network. *Energy AI* **2022**, *7*, 100131. [CrossRef]
19. Yang, L.; Wang, S.H.; Zhang, Y.D. EDNC: Ensemble Deep Neural Network for COVID-19 Recognition. *Tomography* **2022**, *8*, 869–890. [CrossRef]
20. Aversano, L.; Bernardi, M.L.; Cimitile, M.; Pecori, R. Deep neural networks ensemble to detect COVID-19 from CT scans. *Pattern Recognit.* **2021**, *120*, 108135. [CrossRef]
21. Tang, S.J.; Wang, C.J.; Nie, J.T.; Kumar, N.; Zhang, Y.; Xiong, Z.H.; Barnawi, A. EDL-COVID: Ensemble Deep Learning for COVID-19 Case Detection From Chest X-Ray Images. *IEEE Trans. Industr. Inform.* **2021**, *17*, 6539–6549. [CrossRef]
22. Melin, P.; Sánchez, D.; Monica, J.C.; Castillo, O. Optimization using the firefly algorithm of ensemble neural networks with type-2 fuzzy integration for COVID-19 time series prediction. *Soft Comput.* **2021**, *1*, 1–38. [CrossRef] [PubMed]
23. Liu, Z.; Mohammadzadeh, A.; Turabieh, H.; Mafarja, M.; Band, S.; Mosavi, A. A New Online Learned Interval Type-3 Fuzzy Control System for Solar Energy Management Systems. *IEEE Access* **2021**, *9*, 10498–10508. [CrossRef]
24. Qasem, S.; Ahmadian, A.; Mohammadzadeh, A.; Rathinasamy, S.; Pahlevanzadeh, B. A type-3 logic fuzzy system: Optimized by a correntropy based Kalman filter with adaptive fuzzy kernel size. *Inf. Sci.* **2021**, *572*, 424–443. [CrossRef]
25. Cao, Y.; Raise, A.; Mohammadzadeh, A.; Rathinasamy, S.; Band, S.; Mosavi, A. Deep learned recurrent type-3 fuzzy system: Application for renewable energy modeling / prediction. *Energy Rep.* **2021**, *7*, 8115–8127. [CrossRef]
26. Hanandeh, S. Introducing mathematical modeling to estimate pavement quality index of flexible pavements based on genetic algorithm and artificial neural networks. *Case Stud. Constr. Mater.* **2022**, *16*, e0091. [CrossRef]
27. Tam, V.; Butera, A.; Le, K.; Da Silva, L.; Evangelista, A. A prediction model for compressive strength of CO2 concrete using regression analysis and artificial neural networks. *Constr. Build. Mater.* **2022**, *324*, 126689. [CrossRef]
28. Aggarwal, C. *Neural Networks and Deep Learning: A Textbook*, 1st ed.; Springer: Cham, Switzerland, 2018; pp. 1–35.
29. Peng, B.; Tong, L.; Yan, D.; Huo, W. Experimental research and artificial neural network prediction of free piston expander-linear generator. *Energy Rep.* **2022**, *8*, 1966–1978. [CrossRef]
30. Prakarsha, K.; Sharma, G. Time series signal forecasting using artificial neural networks: An application on ECG signal. *Biomed. Signal. Process. Control* **2022**, *76*, 103705. [CrossRef]
31. Gurney, K. *An Introduction to Neural Networks*, 1st ed.; CRC Press: Florida, FL, USA, 1997; pp. 3–10.
32. Haykin, S. *Neural Networks: A Comprehensive Foundation*, 2nd ed.; Prentice Hall: Hoboken, NJ, USA, 1998; pp. 56–75.
33. Zadeh, L. Fuzzy sets. *Inf. Control.* **1965**, *8*, 338–353. [CrossRef]
34. Zadeh, L. The concept of a linguistic variable and its application to approximate reasoning. *Inf. Sci.* **1975**, *8*, 199–249. [CrossRef]
35. Zadeh, L. Some reflections on soft computing, granular computing and their roles in the conception, design and utilization of information/intelligent systems. *Soft Comput.* **1998**, *2*, 23–25. [CrossRef]
36. Melin, P.; Castillo, O. *Hybrid Intelligent Systems for Pattern Recognition Using Soft Computing: An Evolutionary Approach for Neural Networks and Fuzzy Systems*, 1st ed.; Springer: Cham, Switzerland, 2005; pp. 25–40.
37. Al-Jamimi, H.; Saleh, T. Transparent predictive modelling of catalytic hydrodesulfurization using an interval type-2 fuzzy logic. *J. Clean. Prod.* **2019**, *231*, 1079–1088. [CrossRef]
38. Melin, P.; Castillo, O. A review on type-2 fuzzy logic applications in clustering, classification and pattern recognition. *Appl. Soft Comput.* **2014**, *21*, 568–577. [CrossRef]
39. Rickard, J.; Aisbett, J.; Gibbon, G. Fuzzy subsethood for fuzzy sets of type-2 and generalized type-n. *IEEE Trans. Fuzzy Syst.* **2009**, *17*, 50–60. [CrossRef]
40. Mohammadzadeh, A.; Sabzalian, M.; Zhang, W. An Interval Type-3 Fuzzy System and a New Online Fractional-Order Learning Algorithm: Theory and Practice. *IEEE Trans. Fuzzy Syst.* **2020**, *28*, 1940–1950. [CrossRef]
41. Castillo, O.; Castro, J.R.; Melin, P. *Interval Type-3 Fuzzy Systems: Theory and Design*, 1st ed.; Springer: Cham, Switzerland, 2022; pp. 45–67.
42. Yang, X. Firefly algorithms for multimodal optimization. In *Stochastic Algorithms: Foundations and Applications. SAGA 2009. Lecture Notes in Computer Science*, 1st ed.; Watanabe, O., Zeugmann, T., Eds.; Springer: Berlin/Heidelberg, Germany, 2009; Volume 5792, pp. 169–178.

43. Yang, X.; He, X. Firefly Algorithm: Recent Advances and Applications. *Int. J. Swarm Intell. Res.* **2013**, *1*, 36–50. [CrossRef]
44. Chen, Z.; Ashkezari, A.; Tlili, I. Applying artificial neural network and curve fitting method to predict the viscosity of SAE50/MWCNTs-TiO2 hybrid nanolubricant. *Phys. A: Stat. Mech. Appl.* **2020**, *549*, s0378437119321855. [CrossRef]
45. Che, Z.G.; Chiang, T.A.; Che, Z.H. Feed-Forward Neural Networks Training: A comparison Between Genetic Algorithm And Back-Propagation Learning Algorithm. *Int. J. Innov. Comput. Inf. Control* **2011**, *7*, 5839–5850.
46. Gauthier, J.P.; Micheau, P. Feedfoward and feedback adaptive controls for Continuously Variable Transmissions. *IFAC Proc. Vol.* **2012**, *45*, 1460–1465. [CrossRef]
47. An, Y.; Yoo, K.; Na, M.; Kim, Y.S. Critical flow prediction using simplified cascade fuzzy neural networks. *Ann. Nucl. Energy* **2020**, *136*, 107047. [CrossRef]
48. Budak, Ü.; Guo, Y.; Tanyildizi, E.; Şengür, A. Cascaded deep convolutional encoder-decoder neural networks for efficient liver tumor segmentation. *Med. Hypotheses* **2020**, *134*, 109431. [CrossRef] [PubMed]
49. Pulido, M.; Melin, P. Optimization of Ensemble Neural Networks with Type-2 Fuzzy Integration of Responses for the Dow Jones Time Series Prediction. *Intell. Autom. Soft Comput.* **2014**, *20*, 403–418.
50. Sánchez, D.; Melin, P.; Castillo, O. Optimization of modular granular neural networks using a firefly algorithm for human recognition. *Eng. Appl. Artif. Intell.* **2017**, *64*, 172–186. [CrossRef]
51. The Humanitarian Data Exchange (HDX). Available online: https://data.humdata.org/dataset/novel-coronavirus-2019-ncov-cases (accessed on 30 April 2022).
52. Iantovics, L.B.; Kovács, L.; Rotar, C. MeasApplInt—A novel intelligence metric for choosing the computing systems able to solve real-life problems with a high intelligence. *Appl. Intell.* **2019**, *49*, 3491–3511. [CrossRef]